ASSESSING OBSERVER STATIONS FOR CISLUNAR SPACE DOMAIN AWARENESS

THESIS

Michael S. Rosenof, Major, USAF

AFIT-ENY-MS-20-D-068

DEPARTMENT OF THE AIR FORCE
AIR UNIVERSITY

AIR FORCE INSTITUTE OF TECHNOLOGY

Wright-Patterson Air Force Base, Ohio

AFIT-ENY-MS-20-D-068

ASSESSING OBSERVER STATIONS FOR CISLUNAR SPACE DOMAIN AWARENESS

THESIS

Presented to the Faculty

Department of Aeronautics and Astronautics

Graduate School of Engineering and Management

Air Force Institute of Technology

Air University

Air Education and Training Command

In Partial Fulfillment of the Requirements for the

Degree of Master of Science in Astronautical Engineering

Michael S. Rosenof, MS

Major, USAF

December 2020

AFIT-ENY-MS-20-D-068

ASSESSING OBSERVER STATIONS FOR CISLUNAR SPACE DOMAIN AWARENESS

Michael S. Rosenof, MS

Major, USAF

Committee Membership:

Lt Col Bryan D. Little, PhD
Chair

Maj Joshuah A. Hess, PhD
Member

Maj Costantinos Zagaris, PhD
Member

Abstract

With renewed worldwide interest in cislunar space, the need for reliable domain awareness in that extended region of space is clear. This investigation quantifies the suitability of several possible stations for observer satellites in cislunar space by calculating the specific irradiance each would observe as they track satellites in various realistic lunar free-return trajectories across a decade, using reflected sunlight. This investigation includes one class of free return trajectories for target satellites, eleven distinct observer stations, and three different metrics for comparing the effectiveness of each observer station or combination of observer stations for sensing targets using reflected sunlight. The analysis showed that observer satellites in most, but not all, observer stations would be more effective than in low Earth orbit, and certain combinations of observer stations were significantly more effective. The exact ranking of least to most effective varied depending on the metric used.

To my wife and daughters, who tolerated and even encouraged this temporary diversion from them, understanding its significance to my own professional goals and to the needs of the space program; and to my parents, who each separately taught me the sacred value of study, and the utility of technical metrics for solving complex problems

Acknowledgments

I would like to express my sincere gratitude to my faculty advisor, Lt Col Bryan Little, for his guidance and support throughout the course of this thesis effort. As a part time student living two states away, advising me may have presented additional challenges, but Lt Col Little always gave me everything I needed to succeed. He encouraged me to be creative in my approach, and at the same time kept me grounded, extending to me the benefit of an unbroken chain of teachers and students going back to the earliest astronomers. Engineering in general, and Astrodynamics in particular can be seen as a collection of physical laws and analytical tools that together reveal a magic code to the universe, and a formula for manipulating it; for sharing their insight into all of these, I'm deeply grateful to AFIT's entire Astronautical Engineering faculty. I would also like to express my thanks to my Space Operations colleagues and superiors in the burgeoning United States Space Force headquarters, and the Headquarters Air Force more generally, who by welcoming a developmental engineer into their world instilled in me an understanding of space operations capabilities and capability gaps, including with regard to cislunar space.

Michael S. Rosenof

Table of Contents

Page

Abstract iv
Table of Contents vii
List of Figures x
List of Tables xii
I. Introduction 1
Strategic Environment 1
Problem Statement 2
Research Objectives/Hypotheses 3
Research Focus 4
Investigative Questions 4
Methodology 5
Assumptions/Limitations 5
II. Literature Review 6
Chapter Overview 6
Relevant Research 6
Summary 8
III. Methodology 8
Chapter Overview 8
Coordinate Systems 8
Transforming Between Reference Frames 11
Observers 15
Performing the Numerical Integration 20
Determining Initial Conditions 25

Calculating Specific Irradiance 26
Metrics 28
Aggregating Metrics 31
Sensitivity Analysis 32
Summary 33
IV. Analysis and Results 33
Chapter Overview 33
Simulated Orbits 33
Specific Irradiance Calculated 36
Metrics Calculated 38
Metrics Aggregated 41
Results of Sensitivity Analysis 46
General Results 53
Investigative Questions Answered 57
Summary 58
V. Conclusions and Recommendations 59
Chapter Overview 59
Conclusions of Research 59
Significance of Research 60
Recommendations for Action 61
Recommendations for Future Research 61
Summary 64
Appendix A: Derivation of Equation for Location of Earth-Moon L1 65
Appendix B: Full Table of Results 68

Bibliography 71

List of Figures

Page

Figure 1. Earth, Moon, and Relevant Lagrangian Points in ECMF 10

Figure 2. Observer Station #5 Propagated for 6 Hours and 100 Days (all units in km) ... 19

Figure 3. Observer Station #8 Propagated for 6 Hours and 100 Days 20

Figure 4. Example of Metric 1, Comparing L1 and L4 29

Figure 5. Example of Metric 2, Comparing L1 and L4 30

Figure 6. Example of Metric 3, Comparing L1 and L4 31

Figure 7. Sample Target Orbit Plotted in SCI, Full View and Zoomed In 34

Figure 8. Sample Target Orbit Plotted in ECNR 34

Figure 9. Sample Target Orbit Plotted in ECMF 35

Figure 10. Comparison of Target Orbits 15 Days Apart 36

Figure 11. Specific Irradiance Plotted Across One Target Trajectory 37

Figure 12. Specific Irradiance Plotted Across One Target Trajectory, Zoomed in for Emphasis 37

Figure 13. Comparison of Specific Irradiance Curves 15 Days Apart 38

Figure 14. Metric 1 for a Sample Target Orbit 39

Figure 15. Metric 1 for a Sample Target Orbit 40

Figure 16. Metric 3 for a Sample Target Orbit 41

Figure 17. Comparison of Metric 1 for Two Target Orbits 15 Days Apart 42

Figure 18. Comparison of Metric 2 for Two Target Orbits 15 Days Apart 42

Figure 19. Comparison of Metric 3 for Two Target Orbits 15 Days Apart 43

Figure 20. Metric 1 Aggregated Across a Decade 44

Figure 21. Metric 2 Aggregated Across a Decade 45

Figure 22. Metric 3 Aggregated Across a Decade 46

Figure 23. Comparison of Metric 1 With and Without Jupiter's Gravity 47

Figure 24. Comparison of Metric 2 With and Without Jupiter's Gravity 48

Figure 25. Comparison of Metric 3 With and Without Jupiter's Gravity 49

Figure 26. Comparison of Metric 1 Using Two Different Intervals 50

Figure 27. Comparison of Metric 2 Using Two Different Intervals 51

Figure 28. Comparison of Metric 3 Using Two Different Intervals 52

Figure 29. Metric 1 for All 11 Observer Stations 54

Figure 30. Metric 3 for All 11 Observer Stations 54

Figure 31. Metric 1 for All Observer Stations Stationary in ECMF 55

Figure 32. Metric 3 for All Observer Stations Stationary in ECMF 56

List of Tables

Page

Table 1. Observer Stations 18

Table 2. Comparison of Metrics With and Without Jupiter's Gravity 50

Table 3. Comparison of Metrics Using Two Different Intervals 52

Table 4. Metrics Ranked and Scored for All Observer Stations 57

Table 5. Metrics Ranked and Scored for All Observers and Combinations 68

ASSESSING OBSERVER STATIONS FOR CISLUNAR SPACE DOMAIN AWARENESS

I. Introduction

Strategic Environment

Half a century after humanity's debut in cislunar space, multiple spacefaring nations are in friendly competition to operate missions of exploration on and near the Moon. Having succeeded in their first attempt at a lunar mission in 2008 with the Chandrayaan-1 lunar orbiter (Department of Space, Indian Space Research Organisation, 2017), India followed up with a partially successful Chandrayaan-2 mission in 2019, consisting of an orbiter still in operation in November 2020, and a lander and rover that failed to land safely on the surface. The Indian Space Research Organisation has announced its planned second attempt at a lander and rover as part of Chandrayaan-3, likely to be launched in 2021 (Wall, 2020). Israel also plans to follow a lunar mission that fell short of success with a subsequent attempt. After the failure of their Beresheet lunar lander to slow sufficiently for a soft landing on the lunar surface in 2019, Israel's SpaceIL organization announced that it may send a follow-on mission to a different destination in the solar system (Bartels, 2019). China may realize larger lunar ambitions through the use of their Long March 5 heavy lift launch vehicle, which they first tested in November 2016 (Cheng, 2016). It was a much smaller Long March 3B that launched their Chang'e-4 mission in 2018, which landed the Yutu-2, humanity's first probe to the surface of the far side of the Moon (The Planetary Society, 2020). To enable that mission required a communications relay, and to that end, China used an even smaller Long

March 4C to launch the Queqiao relay satellite to a halo orbit around the Earth-Moon L2 Lagrangian point in May 2018 (Xu, 2018). The United States, having completed many notable crewed and robotic missions to the Moon in the past, naturally has more planned for the near future. NASA's Artemis program aims to send the first woman and the next man to the lunar surface by 2024, in order to mature the technologies necessary for the first human presence on Mars (National Aeronautics and Space Administration, 2020). Regardless of whether future activities in the region within the Moon's orbit and sphere of influence remain peaceful, safety of all involved will require reliable domain awareness in cislunar space. US Space Domain Awareness has been focused until now on the regions between low Earth orbit (LEO) and geostationary Earth orbit (GEO).

Problem Statement

Current US national security Space Domain Awareness capabilities are oriented toward observing and tracking objects in Earth orbit between LEO and GEO. Domain awareness throughout the vast volume of space between GEO and the Moon's orbit remains unfulfilled because there has traditionally been little need for it, but with growing interest in cislunar operations, that need is starting to manifest.

The vast distances involved preclude active radar: Since the intensity of radar energy will drop with the inverse square of the distance to the target, and the same will apply to the radar return, the power required to detect an object using radar will increase with the fourth power of distance (Wiesel, Spaceflight Dynamics, 2010). The US Space Force's COBRA DANE radar is an example of a building-sized active radar used to detect and track objects in space in support of the US Space Force's Space Domain

Awareness mission. It is specifically used for tracking objects in LEO (Fact Sheets: COBRA DANE Radar, 2017), at altitudes of only hundreds of kilometers. Given the inverse fourth power relationship between distance and required power, to track the same objects hundreds of thousands of kilometers away, such as would be typical in cislunar space, would require on the order of one trillion times as much energy. Radar, whether operating on the ground or at any particular location in space, would therefore not be suitable for cislunar Space Domain Awareness.

The most promising remaining option is passive optical sensing of reflected sunlight. Given the many options for placement of optical sensors in cislunar space, and with optical sensors currently operating in support of Space Domain Awareness on the ground and in LEO, a study is needed to determine whether any cislunar orbits are more suitable than LEO, and how those options compare.

Research Objectives/Hypotheses

The ultimate objective of this study is to inform Space Domain Awareness mission architecture and planning decisions regarding placement of sensors for optimal detection and tracking of objects in cislunar space, defined here in terms of the quantity of reflected sunlight detectable at a sensor's location. Such sensors would need to be situated and distributed in such a way as to reliably survey vast volumes of space, and detect, track, and maintain custody of objects.

If the effectiveness of an observer station can be measured simply in terms of the quantity of sunlight reflected off a satellite in a circumlunar free return originating at GEO altitudes, detectable at the observer's location, the best observer stations may be in

the vicinity of the Earth-Moon L4 or L5 Lagrangian points, since they are equidistant in the synodic frame between Earth and the Moon. Observer stations in the vicinity of the Moon itself may be even better, since translunar orbits are roughly similar to elliptical Earth orbits, and objects in elliptical orbits spend the majority of their time near apogee; in the case of translunar orbits, this would mean they spend more time near the Moon than Earth, so an observer near the Moon might be most effective.

Research Focus

There are many ways to assess the suitability of an observer station. A method may take into account costs, including the launch cost as a function of delta-V required to reach a particular station, or the cost of a sensor as a function of its aperture area, which itself may be a function of distance to targets. It may instead compare only technical attributes, such as an orbital station's level of reliance on station-keeping. This study will not consider any of those factors, although they may be valuable considerations. Instead, this study will focus only on how the geometry of an observer station will determine its ability to detect objects in specific cislunar orbits using reflected sunlight.

Investigative Questions

This investigation seeks to answer three questions: 1) What general category of orbits would put an observer satellite in the position of observing objects in cislunar space with the greatest brightness of reflected sunlight? 2) How would the suitability of combinations of those categories of orbits compare? 3) What metrics can be used to reliably compare the suitability of different such categories of orbits?

Methodology

To answer the investigative questions, this study utilizes a series of realistic numerically integrated trajectories, modeling the motion of a target satellite in several representative translunar free returns, as well as a set of observer satellites in different orbits.

Irradiance is the measure of incident light that might reach a sensor; for the purposes of this study, it is the amount of light energy available to be collected by a sensor, having been emitted by the Sun, and reflected by a target satellite. Irradiance is a function of the emitted power of the Sun's electromagnetic radiation, the cross-sectional area and optical properties of the target satellite, and the geometry of the Sun, target, and observer.

At regular intervals throughout the trajectories, the portion of the irradiance determined by the geometry is calculated. In order to account for changes in sun angle due to the orbits of the Moon and Earth, each trajectory is repeated at regular intervals across a decade. The irradiance results are transformed into three distinct metrics meant to derive meaning from the irradiance data, and then aggregated across the entire decade. Finally, the metrics of each observer and many meaningful combinations of observers are compared in order to rank observers and combinations of observers from best to worst.

Assumptions/Limitations

This initial study comparing several options for observer stations in cislunar space only addresses the suitability of different stations, not the satellites themselves, so it does not account for the capabilities of actual sensors or of satellites. Two of the observer

stations are stable Earth-Moon Lagrangian points, and one is an unstable Lagrangian point; rather than model realistic orbits around or near these points, this study uses the calculated locations of these points.

There is an infinite variety of orbits a satellite could follow in cislunar space, and the need for domain awareness applies to all of them. This study focuses only on one category of cislunar orbits: circumlunar free returns that originate at GEO, that are coplanar with the Moon's orbit, and that pass between the Moon and Earth.

The precision of an actual orbit determination will depend on the precision and the geometry of observations, so the quality of an observer scheme will improve with the combination of observer stations in multiple locations viewing the same object from very different angles (Wiesel, Modern Orbit Determination, 2010). This study ignores that effect, and addresses only perceived brightness. It also ignores, in general, the theoretical precision of an orbit determination based on observation.

II. Literature Review

Chapter Overview

The purpose of this chapter is to summarize the current state of published research on the topic of Space Domain Awareness in cislunar space.

Relevant Research

Capt Simon Knister, a previous AFIT Systems Engineering MS student, published a thesis that took a systems engineering approach to evaluate systems designed for cislunar space domain awareness. His main goal was to assess the efficacy of systems engineering tools for evaluating cislunar Space Domain Awareness systems, but he also

used those tools to evaluate two such systems. He noted that no papers had been published on electro-optic Space Domain Awareness architectures meant to observe non-cooperative objects in cislunar space. Using the tools he assessed, he compared the cost and effectiveness of different cislunar Space Domain Awareness sensor schemes, but he only considered two, which utilized ground-based sensors and sensors in LEO, and he only considered a target satellite in a quasi-periodic orbit about the Earth-Moon L1 point. He found that of those two observer schemes, the one using sensors in LEO was less expensive and more effective (Knister, 2020).

Jacob K. Vendl performed a study similar to the present one for a master's thesis under Marcus J. Holzinger at the University of Colorado at Boulder in 2020. For observer stations, Vendl considered several families of periodic orbits around the Earth-Moon L1 and L2 points, as well as distant retrograde periodic orbits possessing integer m:n resonance with the Moon's synodic period, and found that several of them performed very well. He used a single metric to evaluate each observer's ability to detect objects using reflected sunlight. He defined a 20° conical right frustum, a cone with its vertex truncated, from the surface of the Earth to the Earth-Moon L2 point, which he asserted adequately approximated the volume of cislunar space. Using realistic characteristics of a sensor and a target satellite, he then calculated what percentage of the total volume of that frustum represented locations where the target satellite would be detectable by the sensor (Vendl, 2020). Vendl's study differed from the present one in three key ways: First, it did not consider actual target satellite orbits, but instead considered the entire volume of cislunar space without regard for how frequently objects may be expected to occupy each point in it; second, it modeled observer stations as actual orbits, rather than

points fixed to the motion of the Moon; third, it used one metric that applied to what was modeled as the entire cislunar domain. Although the means were very different, Vendl's study achieved some of the goals of the present one, using a very different approach.

Summary

Prior to the present study, other very recently published research has investigated different parts of the same problem using very different approaches. To the author's knowledge, none have compared the effectiveness of different observer stations in cislunar space at observing specific objects in cislunar space, but one study did demonstrate that a realistic system of observers in LEO was more effective than a realistic system of ground-based observers, and another demonstrated that observers in certain specific cislunar orbits could very effectively view objects throughout cislunar space. The present study does not attempt to assess *realistic* systems of observers; rather, it assesses the ability of satellites in general categories of observer stations to view objects in other, specific, orbits.

III. Methodology

Chapter Overview

The purpose of this chapter is to describe, in detail, how this study was conducted. All dynamics modeling, data collection, and aggregation was done using MATLAB.

Coordinate Systems

In order to ensure the dynamics are representative of reality, all equations of motion used in the numerical integration of Earth, Moon, Jupiter, target spacecraft, and those observer stations modeled as actual orbits, are defined with respect to an inertial

reference frame. That frame is centered at the solar system's barycenter, and is referred to in this report as "Sun-Centered Inertial," or "SCI." Since the solar system's barycenter is at all times inside the Sun (Wiesel, Spaceflight Dynamics, 2010), and for simplicity, no distinction is made here between that point and the center of the Sun. The orientation of the principal axes in the SCI frame are consistent, but are ultimately of no consequence to this study, since all quantities of interest are calculated based on the relative positions of the Sun, Earth, Moon, Jupiter, targets, and observers, and the orientations of the principal axes in the other two reference frames are defined based on the motion of the Moon and Earth.

A convenient way of displaying translunar orbits might show Earth on the left, the Moon on the right, and the Earth-Moon Lagrangian points fixed, as in Figure 1. That coordinate system is defined here as fixing Earth's location at the origin, fixing the Moon's location at the coordinates (1,0,0), and orienting the 1-2 plane so that the Moon's instantaneous motion in orbit around Earth is tangent to the 1-2 plane with a positive 3-component. That reference frame is defined here as "Earth-Centered, Moon Fixed," or "ECMF," and is akin to the Earth-Moon synodic frame, only translated, since the Earth-Moon synodic frame is centered at the Earth-Moon barycenter.

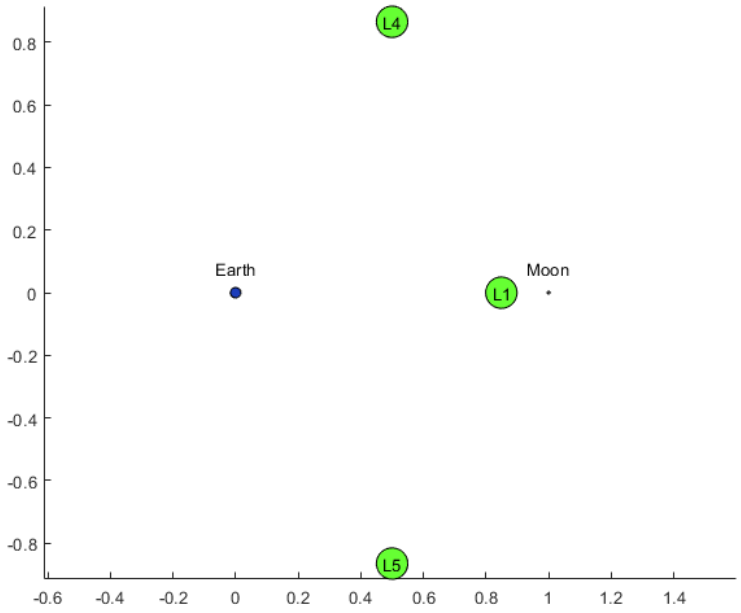

Figure 1. Earth, Moon, and Relevant Lagrangian Points in ECMF

Although not as useful for displaying results, a third reference frame serves primarily as an interim step in transformations between SCI and ECMF. That frame is centered on Earth, but shows the Moon's motion relative to Earth. That reference frame is defined so that the instantaneous motion of the Moon relative to Earth is tangent to the 1-2 plane, and is counterclockwise about the positive 3-axis. By centering on Earth and not rotating, it negates Earth's motion about the Sun. It is useful for displaying the Moon's motion in orbit about Earth, and the motion of any satellite in an orbit coplanar to the Moon's orbit, because it will always confine that motion to the 1-2 plane without any other distortion. It is defined here as "Earth-Centered, Non-Rotating," or "ECNR."

Transforming Between Reference Frames

Transforming between the three aforementioned reference frames is necessary for two reasons: First, the dynamics are most easily modeled in the SCI frame, but plots used for verifying that the trajectories look right are displayed in the ECMF frame; second, the initial conditions for targets and observers are defined in the ECMF frame, but need to be entered into the dynamics in the SCI frame.

A MATLAB function called "SCI_to_ECMF" was devised and is employed to transform position vectors from the SCI frame to the ECMF frame, based on the Earth's and the Moon's state vectors. (There was no need to transform velocities from SCI to ECMF.) It does so through the following steps, illustrated using an object's position vector defined in SCI as $[x \quad y \quad z]^T$, Earth's state vector defined in SCI as $[x_{Earth} \quad y_{Earth} \quad z_{Earth} \quad \dot{x}_{Earth} \quad \dot{y}_{Earth} \quad \dot{z}_{Earth}]^T$, and the Moon's state vector defined in SCI as $[x_{Moon} \quad y_{Moon} \quad z_{Moon} \quad \dot{x}_{Moon} \quad \dot{y}_{Moon} \quad \dot{z}_{Moon}]'$.

Displace the coordinates to be centered at the Earth's center:

$$\begin{bmatrix} x' \\ y' \\ z' \end{bmatrix} = \begin{bmatrix} x - x_{Earth} \\ y - y_{Earth} \\ z - z_{Earth} \end{bmatrix}$$

Scale the resulting vector to make the Earth-Moon distance equal 1:

$$\begin{bmatrix} x'' \\ y'' \\ z'' \end{bmatrix} = \left(\frac{1}{\begin{vmatrix} x_{Moon} - x_{Earth} \\ y_{Moon} - y_{Earth} \\ z_{Moon} - z_{Earth} \end{vmatrix}} \right) \begin{bmatrix} x' \\ y' \\ z' \end{bmatrix}$$

Rotate about the 3-axis to make the Moon appear on the 1-3 plane:

$$\theta = -\tan^{-1}\left(\frac{y_{Moon} - y_{Earth}}{x_{Moon} - x_{Earth}}\right)$$

$$\begin{bmatrix} x''' & x'_{Moon} & \dot{x}'_{Moon} \\ y''' & y'_{Moon} & \dot{y}'_{Moon} \\ z''' & z'_{Moon} & \dot{z}'_{Moon} \end{bmatrix} = \begin{bmatrix} \cos\theta & -\sin\theta & 0 \\ \sin\theta & \cos\theta & 0 \\ 0 & 0 & 1 \end{bmatrix} \begin{bmatrix} x'' & x_{Moon} & \dot{x}_{Moon} \\ y'' & y_{Moon} & \dot{y}_{Moon} \\ z'' & z_{Moon} & \dot{z}_{Moon} \end{bmatrix}$$

Rotate about the 2-axis to make the Moon appear on the 1-axis:

$$\phi = \tan^{-1}\left(\frac{z'_{Moon}}{x'_{Moon}}\right)$$

$$\begin{bmatrix} x'''' & x''_{Moon} & \dot{x}''_{Moon} \\ y'''' & y''_{Moon} & \dot{y}''_{Moon} \\ z'''' & z''_{Moon} & \dot{z}''_{Moon} \end{bmatrix} = \begin{bmatrix} \cos\phi & 0 & \sin\phi \\ 0 & 1 & 0 \\ -\sin\phi & 0 & \cos\phi \end{bmatrix} \begin{bmatrix} x''' & x'_{Moon} & \dot{x}'_{Moon} \\ y''' & y'_{Moon} & \dot{y}'_{Moon} \\ z''' & z'_{Moon} & \dot{z}'_{Moon} \end{bmatrix}$$

Rotate about the 1-axis to make the Moon's motion tangent to the 1-2 plane with a positive 2 component:

$$\psi = -\tan^{-1}\left(\frac{\dot{z}''_{Moon}}{\dot{y}''_{Moon}}\right)$$

$$\begin{bmatrix} x_{ECMF} \\ y_{ECMF} \\ z_{ECMF} \end{bmatrix} = \begin{bmatrix} 1 & 0 & 0 \\ 0 & \cos\psi & -\sin\psi \\ 0 & \sin\psi & \cos\psi \end{bmatrix} \begin{bmatrix} x'''' \\ y'''' \\ z'''' \end{bmatrix}$$

A MATLAB function called “ECMF_to_SCI” was devised and is employed to transform states in the ECMF frame into state vectors in the SCI frame, based on the Earth’s and the Moon’s state vectors, and certain arguments defining an object’s position and velocity in relation to a specified body (Earth or Moon). Those arguments include orbital radius, two angles similar to latitude and longitude, an azimuth angle that defines the direction of the velocity about the local radius vector from the center of the body, and a speed factor that is the multiple of the circular orbit speed. A speed factor of one would produce a circular orbit, absent sufficient perturbing forces to disrupt the circular orbit. Defining a state vector in SCI this way necessarily produces a velocity perpendicular to the local radius vector, but that meets the needs of this study. Latitude, longitude, and

orbital radius in ECMF together define the location part of a state vector in SCI. An angle referred to here as "Latitude" is defined as the angle from the negative 1-axis, and longitude is defined as the angle about the negative 1-axis from the positive 2-axis. Azimuth is defined as the angle of the velocity vector about the local radius, such that it is measured from the positive 2-axis if latitude is zero. The ECMF_to_SCI function transforms states using the following steps, illustrated using an object's position arguments, Earth's state vector defined in SCI as $[x_{Earth} \quad y_{Earth} \quad z_{Earth} \quad \dot{x}_{Earth} \quad \dot{y}_{Earth} \quad \dot{z}_{Earth}]'$, and the Moon's state vector defined in SCI as $[x_{Moon} \quad y_{Moon} \quad z_{Moon} \quad \dot{x}_{Moon} \quad \dot{y}_{Moon} \quad \dot{z}_{Moon}]'$. The position arguments include: orbital radius from the center of the specified body, r; latitude, λ; longitude, ϕ; speed factor, s; and azimuth, γ.

Create the rotation matrix, which is a matrix of the ECMF basis (column) vectors expressed in SCI. The 1-axis basis vector, which is a component of the rotation matrix, is just the unit vector from Earth to the Moon:

$$\overrightarrow{ECMF}_{1,SCI} = \frac{1}{r_{EarthMoon}} \begin{bmatrix} x_{Moon} - x_{Earth} \\ y_{Moon} - y_{Earth} \\ z_{Moon} - z_{Earth} \end{bmatrix}$$

Find the 3-axis basis vector using the cross product of the 1-axis and the Moon's motion relative to Earth, and scaling it to a unit vector:

$$\overrightarrow{ECMF}'_{3,SCI} = \overrightarrow{ECMF}_{1,SCI} \times \begin{bmatrix} \dot{x}_{Moon} - \dot{x}_{Earth} \\ \dot{y}_{Moon} - \dot{y}_{Earth} \\ \dot{z}_{Moon} - \dot{z}_{Earth} \end{bmatrix}$$

$$\overrightarrow{ECMF}_{3,SCI} = \frac{\overrightarrow{ECMF}'_{3,SCI}}{\left|\overrightarrow{ECMF}'_{3,SCI}\right|}$$

Find the 2-axis basis vector using the cross product of the other two:

$$\overrightarrow{ECMF}_{2,SCI} = \overrightarrow{ECMF}_{3,SCI} \times \overrightarrow{ECMF}_{1,SCI}$$

Assemble the rotation matrix:

$$R_{ECMFtoSCI} = \left[\overrightarrow{ECMF}_{1,SCI} \quad \overrightarrow{ECMF}_{2,SCI} \quad \overrightarrow{ECMF}_{3,SCI}\right]$$

Assemble the position vector, starting in ECMF, but scaled, and without accounting for the angles:

$$\vec{r} = \begin{bmatrix} -r \\ 0 \\ 0 \end{bmatrix}$$

Account for the latitude by rotating about the negative 3-axis by the latitude:

$$\overrightarrow{r'} = \begin{bmatrix} \cos(-\lambda) & -\sin(-\lambda) & 0 \\ \sin(-\lambda) & \cos(-\lambda) & 0 \\ 0 & 0 & 1 \end{bmatrix} \vec{r} = \begin{bmatrix} \cos\lambda & \sin\lambda & 0 \\ -\sin\lambda & \cos\lambda & 0 \\ 0 & 0 & 1 \end{bmatrix} \vec{r}$$

Account for the longitude by rotating about the 1-axis by the longitude:

$$\overrightarrow{r''} = \begin{bmatrix} 1 & 0 & 0 \\ 0 & \cos\phi & -\sin\phi \\ 0 & \sin\phi & \cos\phi \end{bmatrix} \overrightarrow{r'}$$

Apply the transport theorem, Equation (1), in order transform the velocity from the ECMF frame to the SCI frame. To do this requires first to find the circular orbital speed in order to convert the speed factor into an actual speed. The steps that follow will assume the reference body is Earth.

$$^{SCI}\dot{\vec{r}}(t) = {}^{ECMF}\dot{\vec{r}}(t) + \vec{\omega}_{ECMF/SCI} \times \vec{r}(t) \tag{1}$$

$$^{ECMF}v = s\sqrt{\frac{\mu_{Earth}}{r}}$$

Assemble and rotate the velocity vector so that it is in the ECMF basis and is referenced with respect to Earth:

$$^{ECMF}\dot{\vec{r}}(t) = \begin{bmatrix} 1 & 0 & 0 \\ 0 & \cos\phi & -\sin\phi \\ 0 & \sin\phi & \cos\phi \end{bmatrix} \begin{bmatrix} \cos\lambda & \sin\lambda & 0 \\ -\sin\lambda & \cos\lambda & 0 \\ 0 & 0 & 1 \end{bmatrix} \begin{bmatrix} 1 & 0 & 0 \\ 0 & \cos\gamma & -\sin\gamma \\ 0 & \sin\gamma & \cos\gamma \end{bmatrix} \begin{bmatrix} 0 \\ ^{ECMF}v \\ 0 \end{bmatrix}$$

Find the angular velocity of the ECMF frame with respect to the SCI frame:

$$\vec{\omega}_{ECMF/SCI} = \frac{1}{r_{EarthMoon}{}^2} \begin{bmatrix} x_{Moon} - x_{Earth} \\ y_{Moon} - y_{Earth} \\ z_{Moon} - z_{Earth} \end{bmatrix} \times \begin{bmatrix} \dot{x}_{Moon} - \dot{x}_{Earth} \\ \dot{y}_{Moon} - \dot{y}_{Earth} \\ \dot{z}_{Moon} - \dot{z}_{Earth} \end{bmatrix}$$

Rotate the angular velocity into the ECMF basis, then apply the transport theorem:

$$^{SCI}\dot{\vec{r}}(t) = {}^{ECMF}\dot{\vec{r}}(t) + \left(R_{ECMFtoSCI}{}^{-1}\vec{\omega}_{ECMF/SCI}\right) \times \overrightarrow{r''}$$

Rotate the velocity vector with respect to the SCI frame into the SCI basis, and account for the velocity of Earth:

$$\begin{bmatrix} \dot{x}_{SCI} \\ \dot{y}_{SCI} \\ \dot{z}_{SCI} \end{bmatrix} = R_{ECMFtoSCI}\, {}^{SCI}\dot{\vec{r}}(t) + \begin{bmatrix} \dot{x}_{Earth} \\ \dot{y}_{Earth} \\ \dot{z}_{Earth} \end{bmatrix}$$

Observers

Fourteen distinct observer stations were modeled, as listed in Table 1. The observer stations labeled "stationary" are stationary in the Earth-Moon synodic frame, and are approximated as stationary in the ECMF frame. They are not modeled as orbits, but rather calculated based on the geometry at any given moment. This includes the unstable Earth-Moon L1 Lagrangian point, and the stable L4 and L5 points, which are defined in the Circular Restricted Three-Body Problem (CR3BP) and displayed in Figure 1, with the Moon and Earth to scale. The CR3BP simplifies the motion of a satellite in a system with two massive bodies by assuming that the motion of the two massive bodies is circular about their mutual barycenter, that they are both point masses, and that the satellite does not affect the motions of the two massive bodies. The five Lagrangian

points are solutions to the CR3BP that are fixed in the frame that rotates with the two massive bodies (Wiesel, Spaceflight Dynamics, 2010). Since the mutual Earth-Moon orbit is roughly circular, and any realistic satellite is much less massive than either body, the CR3BP is a somewhat accurate representation of the Earth-Moon system, and is useful for conceptualizing orbits in cislunar space, but it is not used to model those orbits in the present study. Instead, Earth, Moon, and satellite orbits are numerically integrated in three dimensions using realistic initial conditions, thus not confining the Earth-Moon motion to circular orbits. The locations of L1, L4, and L5 are calculated at each timestep based on an approximation of the instantaneous Earth-Moon motion as circular. Since the CR3BP does not perfectly describe the Earth-Moon system, the Earth-Moon Lagrangian points do not, strictly speaking, exist, but do approximately represent reality. Likewise, their inclusion here, not in the context of the CR3BP, is meant to provide rough locations of quasi-periodic orbits that do exist.

The L4 and L5 points are located at corners of equilateral triangles in the plane of the Moon's motion, preceding and following the Moon, respectively. The L1 point is located on the line between the Moon and Earth, at the point at which the Moon's gravity negates enough of Earth's gravity to enable a circular orbit about Earth closer than the Moon, but with the same orbital period as the Moon (Wiesel, Spaceflight Dynamics, 2010). The location of that point is found analytically based on that principle, and ultimately by numerically solving Equation (2) for D_{L1}. D_{L1} is the distance along the Earth-Moon line from the Moon to L1. The derivation of Equation (2) from Newton's law of universal gravitation and Newton's second law, both expressed along the Earth-Moon axis, is included in Appendix A.

$$\frac{\mu_{Earth}}{(r_{EarthMoon} - D_{L1})^2} = \frac{\mu_{Moon}}{{D_{L1}}^2} + \left(\frac{\mu_{Earth}}{\mu_{Earth} + \mu_{Moon}} r_{EarthMoon} - D_{L1}\right) \frac{\mu_{Earth} + \mu_{Moon}}{{r_{EarthMoon}}^3} \quad (2)$$

There exist quasi-periodic orbits around these Lagrangian points (Wiesel, Spaceflight Dynamics, 2010) that may be of interest to mission planners; the purpose of modeling these points as stationary in the ECMF frame is simply to assess the suitability of the general vicinities of these points and orbits contained within for observer stations. Likewise, Observer Station #4 is the point on the lunar surface facing Earth. This point may actually move slightly relative to the lunar surface throughout the course of the Moon's orbit due to libration, but this is not modeled here, and is assumed not to significantly affect the results. Observer Station #14, the point at 800 km altitude above the point on Earth's surface facing the Moon, is meant to represent the best possible view from LEO, and to a lesser extent, from any ground-based observer. It may approximate the view of a constellation of observer satellites in LEO.

Table 1. Observer Stations

Observer #	Description	Type
1	L1	stationary
2	L4	stationary
3	L5	stationary
4	Moon's nadir point on lunar surface	stationary
5	SV in low circular lunar orbit coplanar with Moon's orbit **(1)**	orbiting
6	SV in same plane as #5, offset by 120°	orbiting
7	SV in same plane as #5, offset by 240°	orbiting
8	SV in low circular lunar orbit in the plane orthogonal to both other planes **(2)**	orbiting
9	SV in same plane as #8, offset by 120°	orbiting
10	SV in same plane as #8, offset by 240°	orbiting
11	SV in low circular lunar orbit in the plane orthogonal to the Earth-Moon vector **(3)**	orbiting
12	SV in same plane as #11, offset by 120°	orbiting
13	SV in same plane as #11, offset by 240°	orbiting
14	notional LEO nadir point at 800 km altitude	stationary

The observer stations labeled “orbiting” are modeled as actual three-dimensional orbits, and determined by numerically integrating the equations of motion. The ones listed are all in low circular lunar orbit, at an orbital radius of 2.2 times the lunar radius. For brevity, the three planes will be referred to by the numbers indicated in bold face. This ensures that a constellation of three satellites evenly distributed across a single plane would all maintain line of sight with each other. Although two satellites may also be used, nominally 180° apart in the same orbit, but offset by the appropriate angle to guarantee they would always maintain line of sight, the combination of three satellites evenly spaced in the same orbit serves as a simple and workable model of the same arrangement. Either would eliminate the susceptibility of a single satellite to eclipsing by the Moon.

The three planes of the satellites in low circular lunar orbit are chosen as mutually orthogonal planes in order to fully envelope the population of possible circular orbits at

that altitude. In reality, to maintain any of those planes would require station-keeping, but maintaining one of those planes may not be necessary, since any real satellite in one of these orbits may be allowed to drift between the three planes. A projection of the trace of the three-dimensional orbit of one such satellite, starting in Observer Station #5, numerically integrated across six hours, and then for contrast, for 100 days, is shown in Figure 2. The contrast seems to indicate the satellite drifts out of its original plane. This model does not account for any asphericity of the Moon, nor of any resulting asymmetry in its gravitation field; that influence would likely serve to only increase the tendency for satellites in low lunar orbit to drift out of their original orbital planes. The actual tendency of these orbital planes to drift is beyond the scope of this study. The aggregation of the results for combinations of these orbits should serve to represent actual constellations in similar orbits.

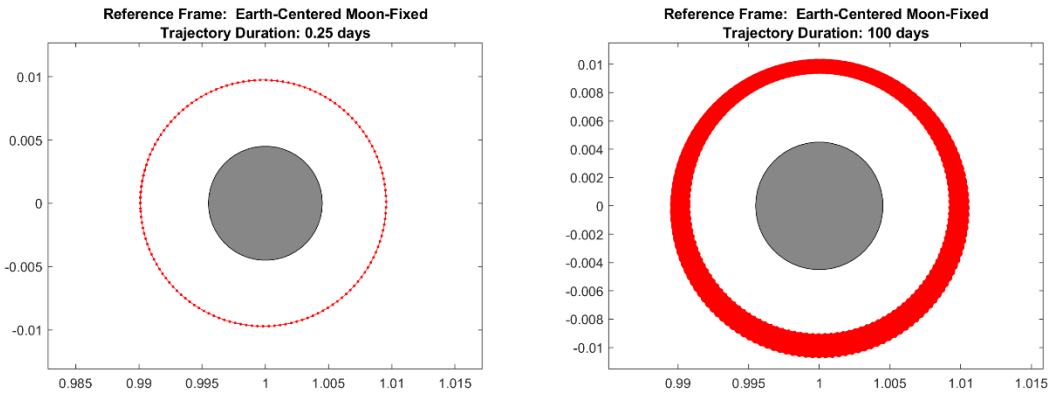

Figure 2. Observer Station #5 Propagated for 6 Hours and 100 Days (all units in km)

To eliminate any doubt that a satellite drifts out of its original plane, the same orbit propagation is repeated for Observer Station #8, whose orbit plane can be viewed on edge in a 1-2 projection in ECMF. This is shown in Figure 3. It should be noted that in these figures, a circle representing the Moon, to scale, is added above the plots of

trajectories, so they do not accurately distinguish when the satellite passes in front of and behind the Moon. In the case especially of the right-hand plot in Figure 3, the profile of the Moon would not be visible otherwise.

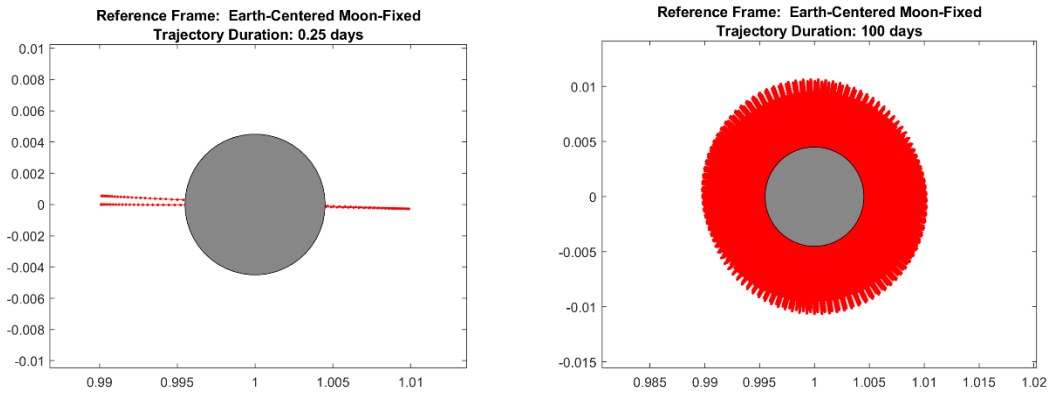

Figure 3. Observer Station #8 Propagated for 6 Hours and 100 Days (all units in km)

Although nine separate low circular lunar orbits are modeled, labeled observer stations #5 through #13 in Table 1, they are not hereafter all treated as distinct. Rather than compare the effectiveness of one satellite against another in the same plane, one satellite (observer stations #5, #8, and #11) is compared to the combination of all three in its own plane.

Performing the Numerical Integration

MATLAB's ode45 function is used to numerically integrate the trajectories of Earth, Moon, Jupiter (when needed), targets, and those observers that are modeled with actual orbits. The equations of motion used are summarized below. The state vector, which includes the states of Earth, Moon, target, observers, and when needed, Jupiter, is defined in Equation (3) along with its first time derivative. Each element of the state vector shown in Equation (3) is actually multiple scalar elements. For example, $\vec{r}_{Earth}$ is actually the three components of Earth's location with respect to the Sun in the SCI

frame, x_{Earth}, y_{Earth}, and z_{Earth}; likewise, $\vec{r}_{Observers\ 1-9}$ is actually the 27 analogous components of the vectors to each of those observers. When Jupiter's influence is included, the state vector has 78 elements; otherwise, it has 72.

$$\vec{X} = \begin{bmatrix} \vec{r}_{Earth} \\ \vec{r}_{Moon} \\ \vec{r}_{Target} \\ \dot{\vec{r}}_{Earth} \\ \dot{\vec{r}}_{Moon} \\ \dot{\vec{r}}_{Target} \\ \vec{r}_{Observers\ 1-9} \\ \dot{\vec{r}}_{Observers\ 1-9} \\ \vec{r}_{Jupiter} \\ \dot{\vec{r}}_{Jupiter} \end{bmatrix}, \quad \dot{\vec{X}} = \begin{bmatrix} \dot{\vec{r}}_{Earth} \\ \dot{\vec{r}}_{Moon} \\ \dot{\vec{r}}_{Target} \\ \ddot{\vec{r}}_{Earth} \\ \ddot{\vec{r}}_{Moon} \\ \ddot{\vec{r}}_{Target} \\ \dot{\vec{r}}_{Observers\ 1-9} \\ \ddot{\vec{r}}_{Observers\ 1-9} \\ \dot{\vec{r}}_{Jupiter} \\ \ddot{\vec{r}}_{Jupiter} \end{bmatrix} \tag{3}$$

The equations of motion that are integrated using ode45 are based on Newton's law of universal gravitation, to include the gravitational influence of the Sun, Earth, Moon, and when needed, Jupiter, on each other and on the target and observers. The gravitational influence of the target and observers on each other is neglected, and all bodies and objects are modeled as point masses for simplicity. This means the perturbing effects of the asphericity of the Earth and Moon are neglected. To integrate these equations of motion, ode45 requires a function that takes the state vector as input and returns its first time derivative. That purpose-built function does so, notionally, by first calculating the component of each object's acceleration vector that is caused by the gravitational influence of each other body, splitting that into components in the 1-, 2-, and 3-axes of the SCI frame, then summing them along each axis for each body or object. For example, the magnitude of the component of Earth's acceleration that is caused by

the Sun-Earth gravitational attraction, $a_{Earth,\,SunEarth}$, is given in Equation (4), where μ_{Sun} is the Sun's gravitational parameter, the product of its mass and the universal gravitational constant, and $r_{SunEarth}$ is the scalar distance from the Sun to Earth. The fully assembled second time derivative of the vector from the Sun to Earth is given in Equation (5). To split each acceleration component into 1-, 2-, and 3-axis components, it is multiplied by the ratio of the signed component of the position vector (e.g., $x_{SunEarth}$, essentially a 1-dimensional position vector taken along the Sun-Earth vector, consisting of a magnitude and a sign, positive or negative, and equivalent to $x_{Earth} - x_{Sun}$) to the magnitude of the position vector (e.g., $r_{SunEarth}$). Since the gravitational force is attractive, the acceleration must always be in opposition to the position vector, so the terms are all negative.

$$a_{Earth,\,SunEarth} = \frac{\mu_{Sun}}{r^2{}_{SunEarth}} \tag{4}$$

$$\ddot{\vec{r}}_{Earth} = \begin{bmatrix} -\frac{a_{Earth,\,SunEarth} x_{SunEarth}}{r_{SunEarth}} - \frac{a_{Earth,\,EarthMoon} x_{MoonEarth}}{r_{EarthMoon}} - \frac{a_{Earth,\,JupiterEarth} x_{JupiterEarth}}{r_{JupiterEarth}} \\ -\frac{a_{Earth,\,SunEarth} y_{SunEarth}}{r_{SunEarth}} - \frac{a_{Earth,\,EarthMoon} y_{MoonEarth}}{r_{EarthMoon}} - \frac{a_{Earth,\,JupiterEarth} y_{JupiterEarth}}{r_{JupiterEarth}} \\ -\frac{a_{Earth,\,SunEarth} z_{SunEarth}}{r_{SunEarth}} - \frac{a_{Earth,\,EarthMoon} z_{MoonEarth}}{r_{EarthMoon}} - \frac{a_{Earth,\,JupiterEarth} z_{JupiterEarth}}{r_{JupiterEarth}} \end{bmatrix} \tag{5}$$

When Jupiter's gravitational influence is included, the terms equivalent to Equation (5) for the Moon and Jupiter also have three components each, but for the target and observers, which are subject to the gravitational influence of four rather than three bodies, there are four terms. Equation (6) shows the fully assembled second time derivative of the vector from the Sun to Observer 1, and serves as an example. When

Jupiter's gravitational influence is not included, all terms related to Jupiter are omitted; in that case, Equation (5) has only two terms in each component, and (6) has three.

$$\ddot{\vec{r}}_{Ob1} = \begin{bmatrix} -\frac{a_{Ob1,\,SunOb1}x_{SunOb1}}{r_{SunOb1}} - \frac{a_{Ob1,\,EarthOb1}x_{EarthOb1}}{r_{EarthOb1}} - \frac{a_{Ob1,\,MoonOb1}x_{MoonOb1}}{r_{MoonOb1}} - \frac{a_{Ob1,\,JupiterOb1}x_{JupiterOb1}}{r_{JupiterOb1}} \\ -\frac{a_{Ob1,\,SunOb1}y_{SunOb1}}{r_{SunOb1}} - \frac{a_{Ob1,\,EarthOb1}y_{EarthOb1}}{r_{EarthOb1}} - \frac{a_{Ob1,\,MoonOb1}y_{MoonOb1}}{r_{MoonOb1}} - \frac{a_{Ob1,\,JupiterOb1}y_{JupiterOb1}}{r_{JupiterOb1}} \\ -\frac{a_{Ob1,\,SunOb1}z_{SunOb1}}{r_{SunOb1}} - \frac{a_{Ob1,\,EarthOb1}z_{EarthOb1}}{r_{EarthOb1}} - \frac{a_{Ob1,\,MoonOb1}z_{MoonOb1}}{r_{MoonOb1}} - \frac{a_{Ob1,\,JupiterOb1}z_{JupiterOb1}}{r_{JupiterOb1}} \end{bmatrix} \quad (6)$$

The calculation of second derivative components thus far described is sound, but Equations (4) and (5), or their equivalents, each involve a division, which is relatively computationally demanding. To make the computation more efficient, r^3 terms are calculated, and the two divisions are combined into one, as shown in Equations (7) and (8), which are analogous to Equations (5) and (6), respectively. Using this method, the computing time was observed to reduce by approximately 20%.

$$\ddot{\vec{r}}_{Earth} = \begin{bmatrix} -\frac{\mu_{Sun}x_{SunEarth}}{r^3_{SunEarth}} - \frac{\mu_{Moon}x_{MoonEarth}}{r^3_{EarthMoon}} - \frac{\mu_{Jupiter}x_{JupiterEarth}}{r^3_{JupiterEarth}} \\ -\frac{\mu_{Sun}y_{SunEarth}}{r^3_{SunEarth}} - \frac{\mu_{Moon}y_{MoonEarth}}{r^3_{EarthMoon}} - \frac{\mu_{Jupiter}y_{JupiterEarth}}{r^3_{JupiterEarth}} \\ -\frac{\mu_{Sun}z_{SunEarth}}{r^3_{SunEarth}} - \frac{\mu_{Moon}z_{MoonEarth}}{r^3_{EarthMoon}} - \frac{\mu_{Jupiter}z_{JupiterEarth}}{r^3_{JupiterEarth}} \end{bmatrix} \quad (7)$$

$$\ddot{\vec{r}}_{Ob1} = \begin{bmatrix} -\frac{\mu_{Sun}x_{SunOb1}}{r^3_{SunOb1}} - \frac{\mu_{Earth}x_{EarthOb1}}{r^3_{EarthOb1}} - \frac{\mu_{Moon}x_{MoonOb1}}{r^3_{MoonOb1}} - \frac{\mu_{Jupiter}x_{JupiterOb1}}{r^3_{JupiterOb1}} \\ -\frac{\mu_{Sun}y_{SunOb1}}{r^3_{SunOb1}} - \frac{\mu_{Earth}y_{EarthOb1}}{r^3_{EarthOb1}} - \frac{\mu_{Moon}y_{MoonOb1}}{r^3_{MoonOb1}} - \frac{\mu_{Jupiter}y_{JupiterOb1}}{r^3_{JupiterOb1}} \\ -\frac{\mu_{Sun}z_{SunOb1}}{r^3_{SunOb1}} - \frac{\mu_{Earth}z_{EarthOb1}}{r^3_{EarthOb1}} - \frac{\mu_{Moon}z_{MoonOb1}}{r^3_{MoonOb1}} - \frac{\mu_{Jupiter}z_{JupiterOb1}}{r^3_{JupiterOb1}} \end{bmatrix} \quad (8)$$

The numerical integration is allowed to continue for the duration of the target's free return, terminating when it reaches its closest approach to Earth, or aborting if it

collides with the Moon or Earth. An event function is used to achieve this. A closest approach to Earth is detected when the target's distance from Earth stops decreasing and starts increasing; the integration then stops, and the results are recorded. A collision is detected when the distance to the Moon or Earth is less than or equal to that body's nominal radius; when that happens, the integration is aborted, the data from that run is discarded, and a message reporting this collision is displayed on the command prompt.

Rather than use ode45 to integrate across the entire trajectory at once, determining a variable timestep itself, a constant timestep of 150 seconds is defined, and ode45 is made to numerically integrate from timestep to timestep. Units of seconds are used, rather than non-dimensional time. Within each 150 second timestep, ode45 numerically integrates from beginning to end, determining its own variable timestep within those 150 seconds, but the trajectory it calculates is discarded, and only the state at the end of each 150 second timestep is recorded. This produces a trajectory array with elements spaced at regular intervals. Integration tolerances of 1.5×10^{-6} (relative) and 1.5×10^{-9} (absolute), which are eight and eleven orders of magnitude smaller than the timestep, were used.

This numerical integration is repeated at regular intervals throughout the 2025-2035 decade in order to establish a representative population of Sun/Earth/Moon configurations. A 150-second timestep was chosen somewhat arbitrarily: It was small enough to produce a large enough data set, as well as a relatively smooth trajectory; and it was large enough so each trajectory run took no longer than 12 hours.

Determining Initial Conditions

The initial conditions of planetary bodies, including Earth, Moon, and Jupiter, are established using MATLAB's planetEphemeris function, which uses the Chebyshev coefficients provided by NASA's Jet Propulsion Laboratory (JPL) (MathWorks, 2020). JPL produces that data based on precise observations of the motion of bodies in the solar system, combined with numerical integration of the equations of motion, which account for the gravitation influence of all major Solar System bodies, and account for each one's asphericity. The planetEphemeris function allows the use of any of several versions of JPL's Development Ephemeris (DE) package, but the commonly used DE405 package produced by JPL in 1997, which is the MATLAB function's default choice, suited the needs of this study. Subsequent DE versions include the influence of a greater number of bodies, such as DE421, which includes the influence of 343 asteroids in the main asteroid belt, but this is far more precision than would be needed to establish realistic initial conditions for the Moon and Earth for use in modeling cislunar trajectories (Jet Propulsion Laboratory, 2014). Since the dynamics are modeled in a Sun-centered reference frame, the Sun's coordinates are always set in that frame as (0,0,0), and all other coordinates are defined in relation to the Sun's location.

The initial conditions for the target satellite are set using the ECMF_to_SCI function and a second purpose-built function, best_latitude2, which finds the latitude initial condition that will generate the most symmetric free return, with respect to the Earth-Moon axis. This is a low-fidelity one-variable optimization. The speed factor initial condition was found by trial and error for each class of free returns. A two-variable optimization, and one of higher fidelity, that determines the optimal latitude and

speed factor to achieve a symmetric free return with a specified perilune distance may be useful for subsequent research, but the present intent is to model a representative population of free returns, not the same free return many times. The one-variable optimization produces free returns with varying perilune distances, so it meets the needs of the present study. The best_latitude2 function uses such an optimization, but does so with a simple walk, varying the latitude by a specified constant amount each try. This may not produce a perfectly symmetric free return, but it meets the needs of the study.

The initial conditions of the orbiting observers are also established using the ECMF_to_SCI function, but using the Moon as the body of reference.

Calculating Specific Irradiance

At any given moment, the location of a target satellite in relation to the Sun, Earth, Moon, and observer will produce an irradiance at the observer that depends on the irradiance of the Sun, the area of the observer's sensor, and its optical properties. That irradiance is given in Equation (9) (Hecht, 2016).

$$I = I_{sun}\frac{A}{r^2}\frac{2}{3}\frac{C_d}{\pi}(\sin\alpha + (\pi - \alpha)\cos\alpha) \tag{9}$$

Where:

I = Irradiance
A = Cross-section area of the optical sensor
r = Distance from Target to Observer
C_d = Coefficient of diffuse reflection
α = Angle from the Sun to Target to Observer

Since the properties of the Sun, and the particulars of the observer satellite are beyond the scope of this investigation, a *specific* irradiance that negates their effect serves as a more relevant figure of merit. That specific irradiance, I^*, is given in Equation (10).

$$I^* = \frac{3}{2}\pi \frac{I}{I_{sun} A C_d} = \frac{sin\,\alpha + (\pi - \alpha)\,cos\,\alpha}{r^2} \tag{10}$$

This specific irradiance is a function only of geometry, and serves as a suitable figure of merit for comparing the effectiveness of different observer stations. For the purposes of this analysis, it is measured in units of km^{-2}. This produces very small values of specific irradiance, raising the possible concern that machine precision may artificially limit the analysis, but the results did not suggest this. It should be noted that since the I_{sun} term is removed from the expression in Equation (10), the calculation of I^* would be no different in a different solar system. This is acceptable because the intent of this study is to compare observer stations, not to establish an accurate absolute performance metric.

The calculation of specific irradiance accounts for four conditions in which an observer would not be able to observe a target satellite due to obscuration or other interference by the Sun, Earth, or Moon: Target is eclipsed by Earth or Moon, so no sunlight can reflect off the target satellite; Earth or Moon is in between target and observer, so observer can't see target; target is between observer and Earth or Moon, so Earth or Moon is in the background of target, thus obscuring the view; and target is between observer and Sun, so observer would have to look directly at the Sun to see target. When any of those conditions are met, the model sets the specific irradiance to zero.

After the numerical integration is complete, the specific irradiance is calculated for each observer and combination of observers at each timestep. The specific irradiance

for a combination of observers is simply the greatest value of specific irradiance from among those observers at that moment.

Metrics

The specific irradiance may serve as a suitable figure of merit, but with a different value at each timestep and within each numerically integrated free return, it must be condensed into some other figure representing an overall trend. Three metrics are defined and used for this purpose, and are aggregated across all of the trajectories modeled across the decade of interest. In the two cases in which it would be meaningful, the metric is aggregated across runs separately as an average value, a minimum value, and a maximum value achieved. These form three separate curves.

Metric 1 is the percentage of times the specific irradiance is greater than or equal to a certain threshold value, as a function of the threshold. As an example, a plot comparing Metric 1 for two different observer stations is shown in Figure 4. In this case, the interval is 25 days. For Metric 1, the higher curve is better. The “average” curve is solid, while the “minimum” and “maximum” curves are shaded.

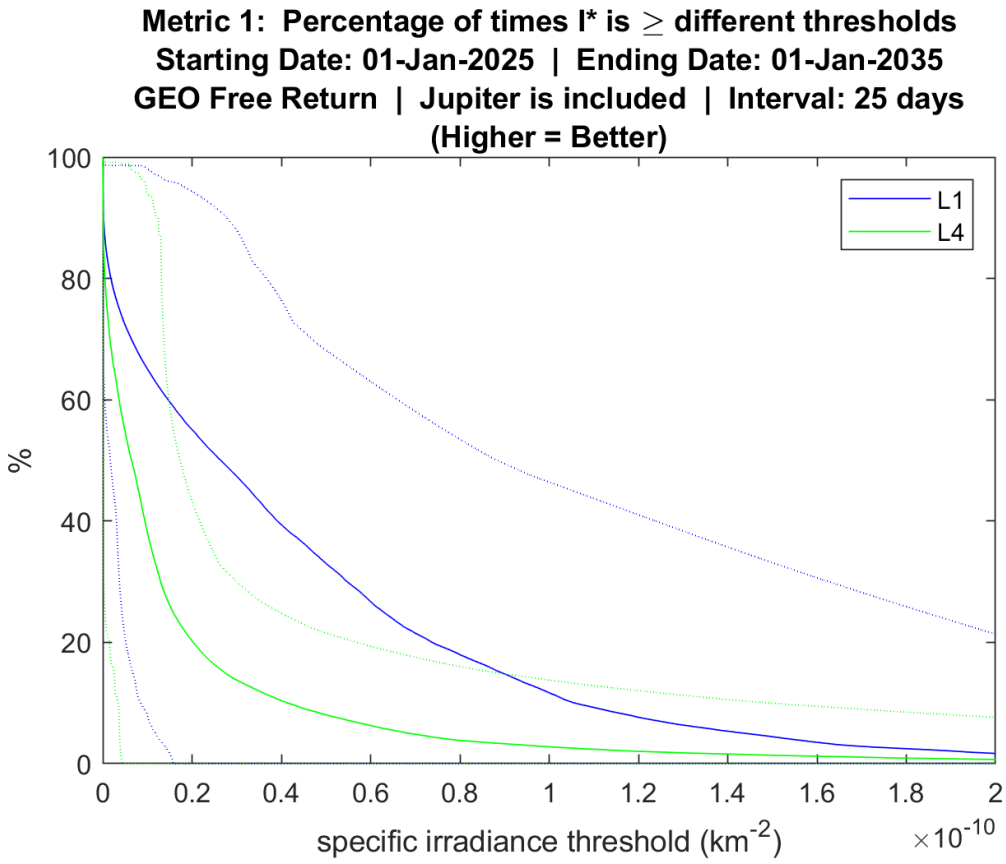

Figure 4. Example of Metric 1, Comparing L1 and L4

Metric 2 is the worst specific irradiance at each point in a normalized trajectory. Even within the same type of free return, the trajectory's duration can vary. In order to calculate Metric 2, the entire trajectory, terminating when the target satellite returns to Earth and reaches its closest approach, is normalized into a duration of 1000 time units. At each time unit, the specific irradiance is interpolated from the actual data. Across runs, the lowest value at each normalized timestep is recorded. An example of the result can be seen in Figure 5, again describing the same pair of observers, and with an interval of 25 days. In this case also, the higher curve is better.

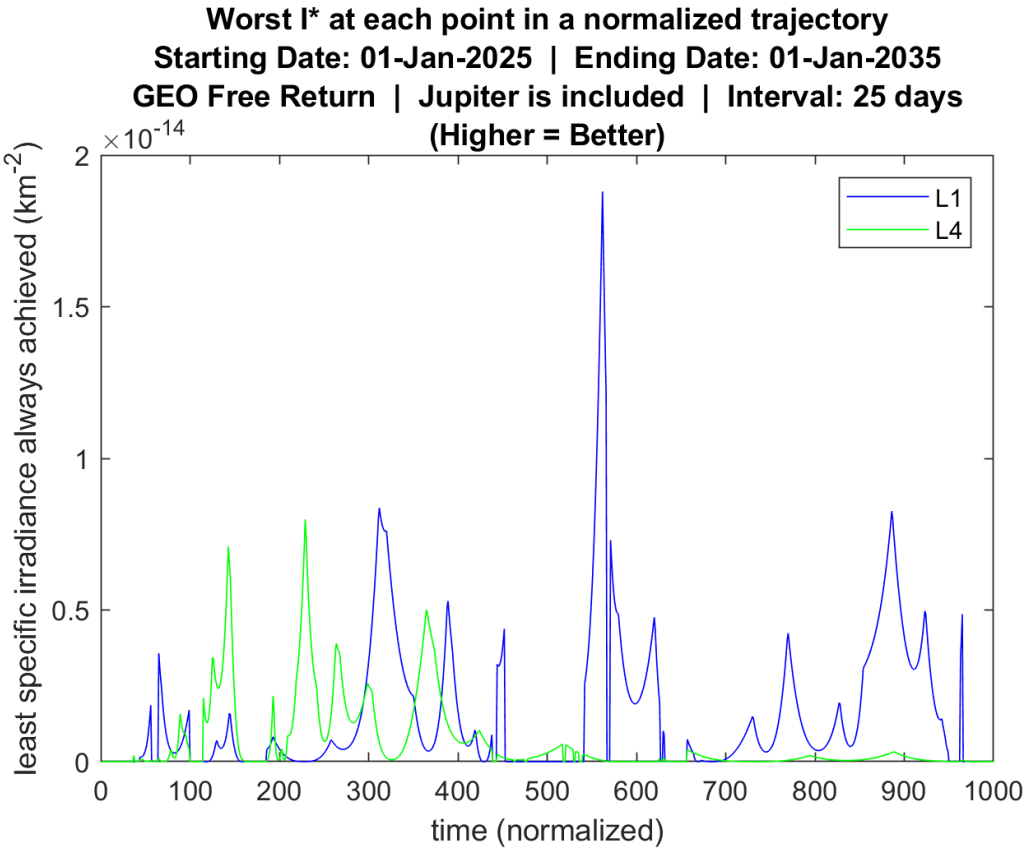

Figure 5. Example of Metric 2, Comparing L1 and L4

Metric 3 is the maximum time required to see a particular value of specific irradiance, as a function of that value. An example plot comparing Metric 3 for the same two observers, and with the same interval, appears in Figure 6. "Average," "Minimum," and "Maximum" curves are again included, and in this case, the lower curve is better.

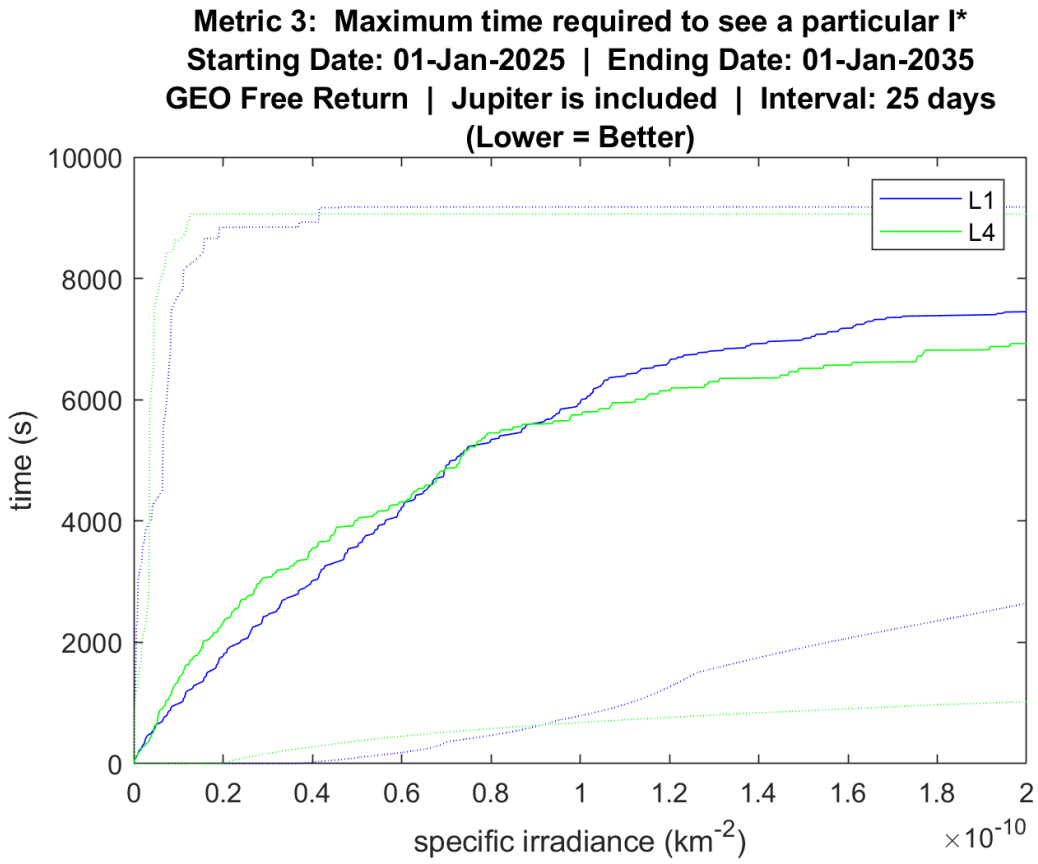

Figure 6. Example of Metric 3, Comparing L1 and L4

Aggregating Metrics

The metrics aggregate the specific irradiances calculated throughout each trajectory run, but in order to rank observers and combinations of observers generally, the metrics need to be aggregated further. By plotting a metric for two different observers in the same plot, it can be clearly seen which observer is better at each point, but to establish that one observer is better than another *overall* would require intelligently weighing the value of each of those points. In the absence of such insight, one observer is judged here to be better than another with respect to a particular metric if its average value is greater than the other's average value (or less than, in the case of Metric 3). The actual average need not be calculated, and the sum of values is used instead, eliminating the need to

divide both sums by the same number of points. The MATLAB function sortMetrics was built and is used for this purpose. It utilizes the data file produced by the main script, SunEarthMoonFRTargetObservers_decade.m, and produces a comma-delimited file ranking all observers and combinations of observers.

Sensitivity Analysis

In order to ensure the results are not biased by numerical artifacts, nor errors in the dynamics, the model was modified in two different ways as part of a sensitivity analysis.

For the results to be believable, the trajectories of Earth, Moon, target, and those observers representing realistic orbits had to be realistic. The model incorporated the gravity of the Sun, Earth, and Moon, but did not include the influences of the other planetary bodies, nor of the asphericity of any gravitational fields. Given the distances involved, any errors in the model due to exclusion of the asphericity of gravitational fields are assumed to be insignificant, but errors due to gravitational influences of bodies other than the Sun, Earth, and Moon were surrogated by adding Jupiter's gravity to the model. The same runs were repeated with and without inclusion of Jupiter's gravity in order to demonstrate that including Jupiter did not change the results.

The intent in repeating the same target and observer trajectories at regular intervals across a decade was to determine how effective each observer was at detecting reflected sunlight across the full range of realistic Sun-Earth-Moon geometric arrangements. If the interval used struck a resonance with the Moon's orbit, then the analysis would fail to model a realistic population of Sun-Earth-Moon geometric

arrangements. In order to minimize the possibility of falling into such a resonance, the entire analysis was repeated with two different intervals that, when expressed in days, share no prime factors: 25 days and 19 days.

Summary

The methodology used in this analysis was designed to accurately model the dynamics of the cislunar region, make simplifying assumptions about the trajectories of certain categories of observer stations, objectively compare the effectiveness of the observer stations, and eliminate the possibility that the results were biased by dynamical or numerical errors.

IV. Analysis and Results

Chapter Overview

This chapter reports the four metrics calculated and aggregated across the decade of interest.

Simulated Orbits

The decade of interest, across which target satellites' lunar free return trajectories were modeled every 19 or 25 days, was January 1, 2025 through January 1, 2035. The first such orbit, departing Earth from a GEO-class altitude of 35,786 km on January 1, 2025, is shown in the SCI, ECNR, and ECMF frames, in Figure 7, Figure 8, and Figure 9, respectively. The red line, labeled "Object" represents the motion of the target satellite. When fixed in the given frame, the Sun, Earth, and Moon are drawn to scale as yellow, blue, and gray circles, respectively. Figure 7 shows that complex motion in the Earth-

Moon system is difficult to resolve in the SCI frame, whereas Figure 8 and Figure 9 show that the ECNR and ECMF frames make it much easier. Figure 8 demonstrates that the target satellite's orbit is approximately elliptical.

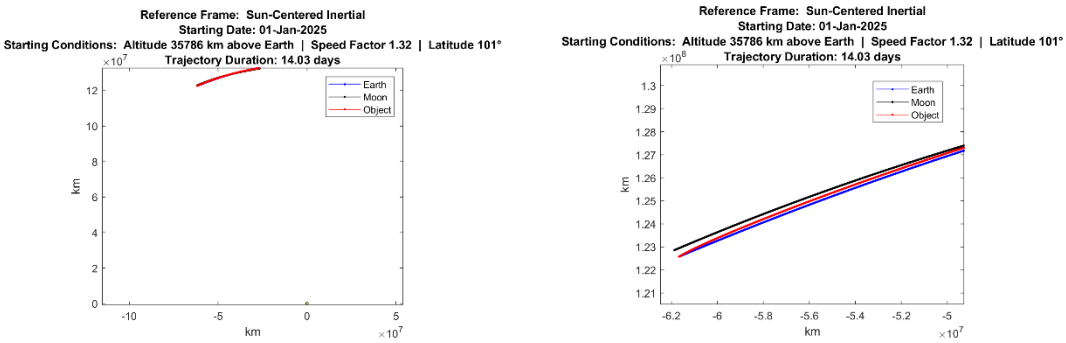

Figure 7. Sample Target Orbit Plotted in SCI, Full View and Zoomed In

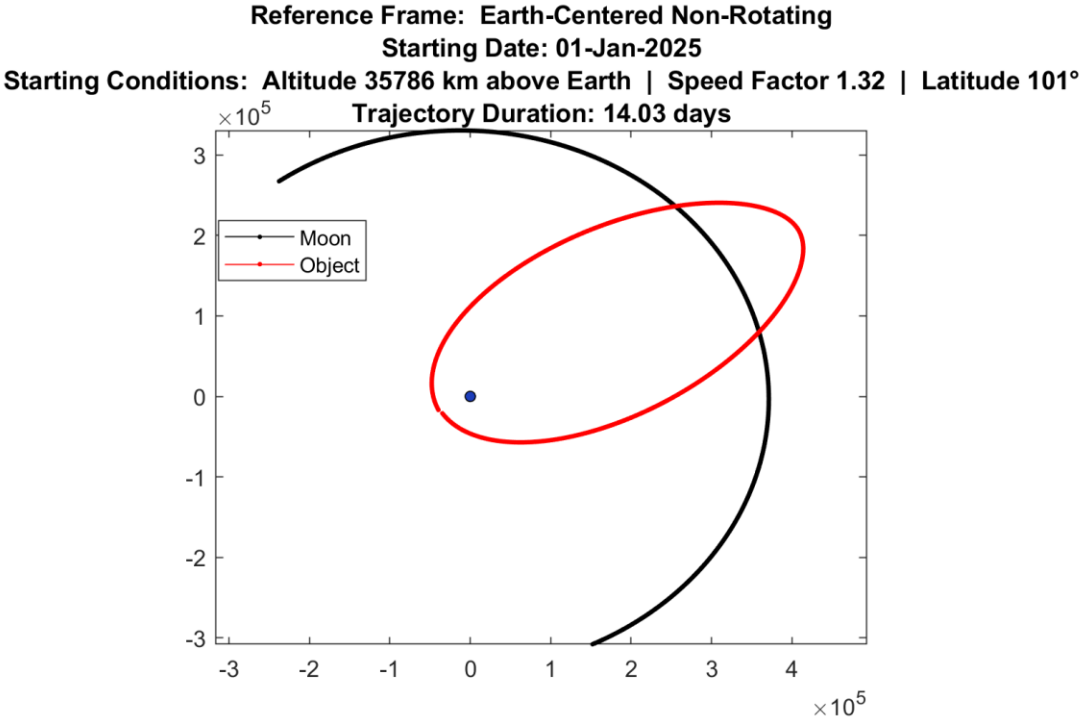

Figure 8. Sample Target Orbit Plotted in ECNR

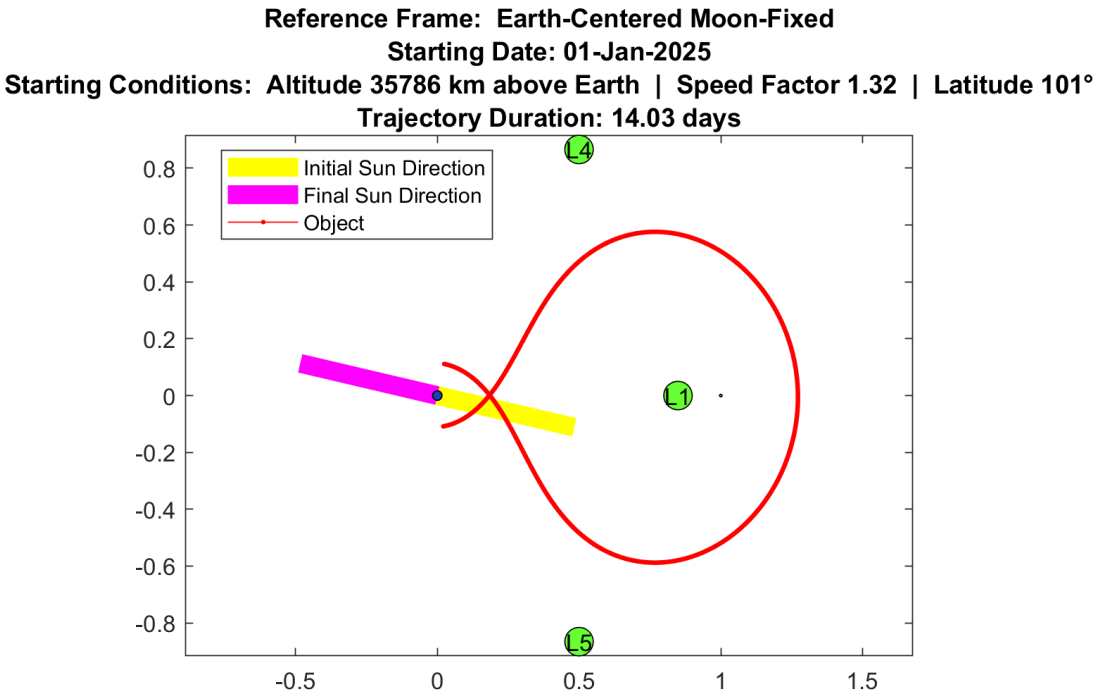

Figure 9. Sample Target Orbit Plotted in ECMF

In order to demonstrate how the target orbit differs when the starting date is changed, the same plot is shown in Figure 10 alongside its counterpart for the same trajectory beginning 15 days later. Both plots indicate the direction of the Sun, projected onto the ECMF frame's 1-2 plane, at the beginning and end of the trajectory, which lasted approximately two weeks. Of note, the Sun may appear to traverse almost 180° in that plane during those two weeks, while Earth would not have passed one tenth of that angle in its orbit. This is due to the rotation of the ECMF frame, which follows the orbit of the Moon: A satellite's two week orbit would coincide with approximately half of an orbit by the Moon, so the initial and final orientations of the Sun in the ECMF frame would be approximately 180° separated, and the same orbit reproduced two weeks later would show those Sun orientations reversed. Both effects are apparent in Figure 10.

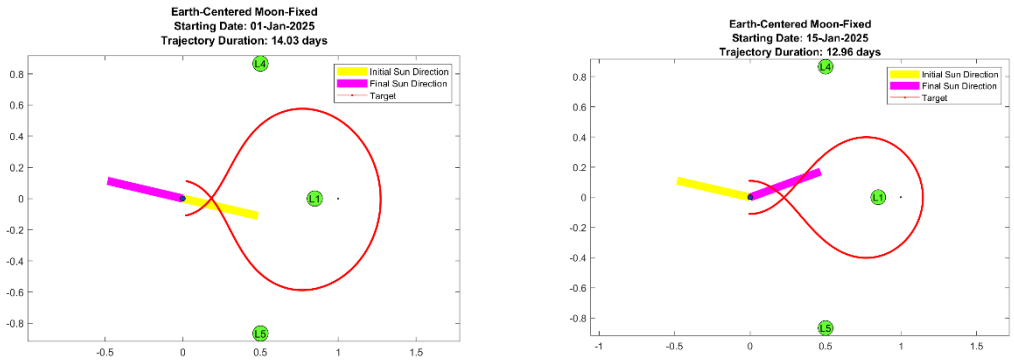

Figure 10. Comparison of Target Orbits 15 Days Apart

Specific Irradiance Calculated

The specific irradiance taken at each of the 11 observer stations across the first simulated orbit, a circumlunar free return from GEO beginning January 1, 2025, is plotted in Figure 11, and again in Figure 12, zoomed in for emphasis. This is plot is meant simply to demonstrate the appearance of the specific irradiance curves for a single trajectory, and to serve as validation that the calculated figures reflect reality. For example, the curve for the observer at L4 peaks early, and the curve for the observer at L5 peaks late and higher, since the Sun angle is better at L5's peak; the curve for an observer at a notional LEO nadir point peaks much higher than the others at the very beginning and the very end of the trajectory, and near the end drops to zero for the brief period when its view is blocked by Earth; the curves for observer stations in low lunar orbit show an oscillation, corresponding to their orbits, and the ones representing single satellites periodically drop to zero as their views are blocked by the Moon.

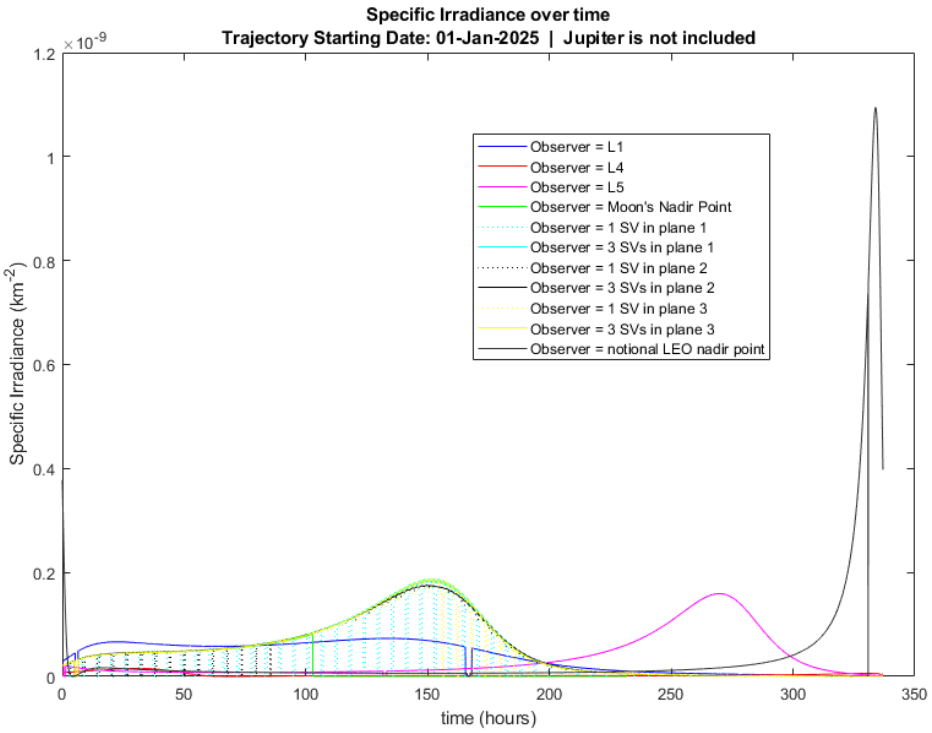

Figure 11. Specific Irradiance Plotted Across One Target Trajectory

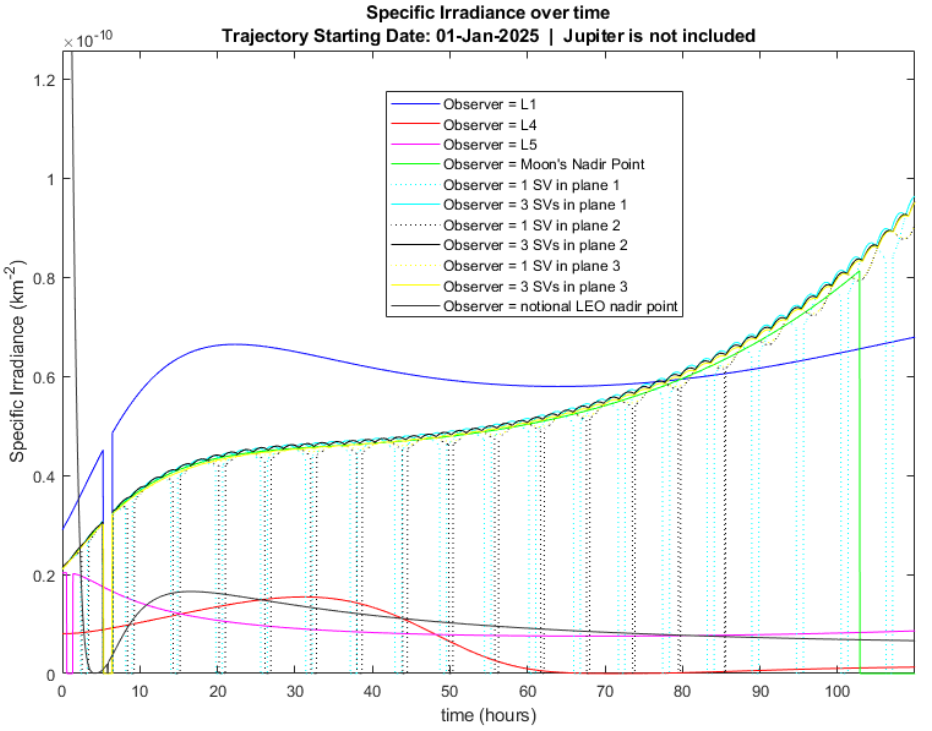

Figure 12. Specific Irradiance Plotted Across One Target Trajectory, Zoomed in for Emphasis

In order to demonstrate how the specific irradiance curves differ when the target trajectory is different, the same plot is shown in Figure 13 alongside its counterpart for the same trajectory beginning 15 days later. It should be noted that the vertical axis scales are not the same. This demonstrates that the individual specific irradiance curves will differ greatly when the trajectory is initiated at different times, and it demonstrates how little insight into the general effectiveness of an observer station such individual specific irradiance curves would offer.

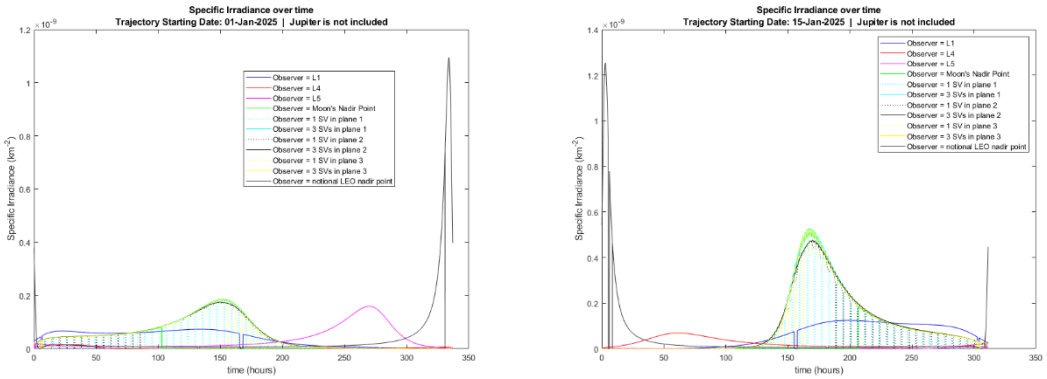

Figure 13. Comparison of Specific Irradiance Curves 15 Days Apart

Metrics Calculated

The specific irradiance at any given moment may be less important than the specific irradiance trend throughout a target trajectory. Those metrics are shown below, aggregating specific irradiance figures throughout the trajectory. Metric 1, *percentage of times specific irradiance is greater than or equal to different thresholds*, is shown in Figure 14. In the same way the specific irradiance curves vary greatly with different starting times, the metrics should vary as well; therefore, none of the curves in Figure 14 should be taken as indicative of an observer station's overall effectiveness. For this particular trajectory, however, Figure 14 can serve to validate Metric 1: For example.

each of the curves should indicate 0% when the specific irradiance threshold reaches the maximum value the specific irradiance actually reaches; for the observer station at L5, this happens at about 1.6×10^{-10} km^{-2}, which is the maximum value indicated in Figure 11.

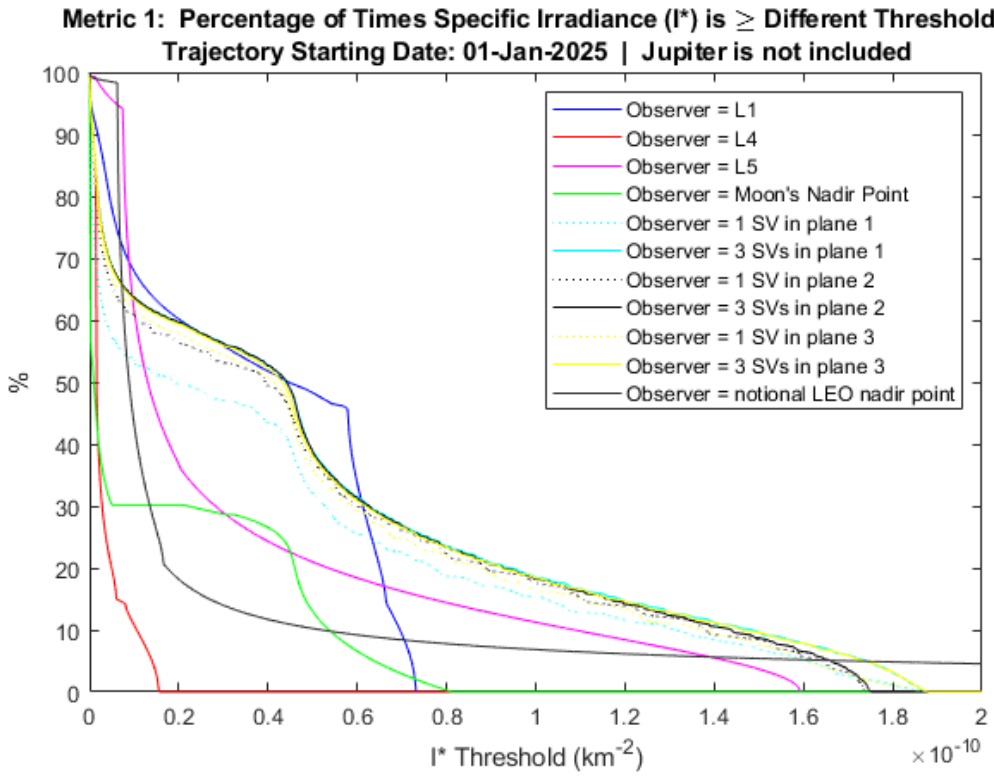

Figure 14. Metric 1 for a Sample Target Orbit

Metric 2, *worst specific irradiance at each point in a normalized trajectory*, for the same target trajectory, is shown in Figure 15. The same stipulation, that this plot is not indicative of observer stations' general effectiveness, applies. Since Metric 2 applied to a single trajectory is simply the specific irradiance curves scaled to 1000 dimensionless time units, it should, and does, appear identical in form to Figure 11.

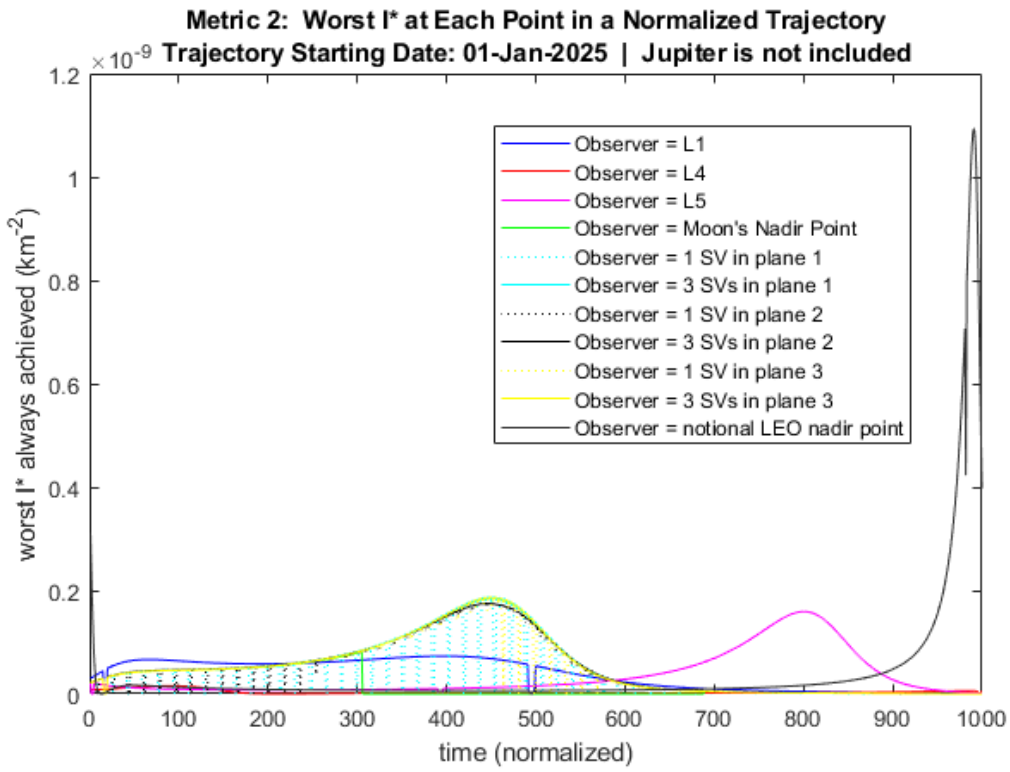

Figure 15. Metric 1 for a Sample Target Orbit

Metric 3, *maximum time required to see a particular irradiance*, for the same trajectory, is shown in Figure 16. The same stipulation regarding applicability once again applies, but this plot can again serve to validate Metric 3: For each observer station, the curve must start at the origin, since no time must pass before a specific irradiance of zero is observed; further, the point at which each curve reaches its peak must reflect the total duration of the trajectory and the maximum specific irradiance measured. In both ways, the plots in Figure 16 behave as expected; for example, the curve representing an observer at L5 starts at the origin and reaches its peak at just over 1.6×10^{6} seconds, which is consistent with the ~14 days indicated for this trajectory in Figure 9, and 1.6×10^{-10} km^{-2}, which again is the maximum value indicated in Figure 11.

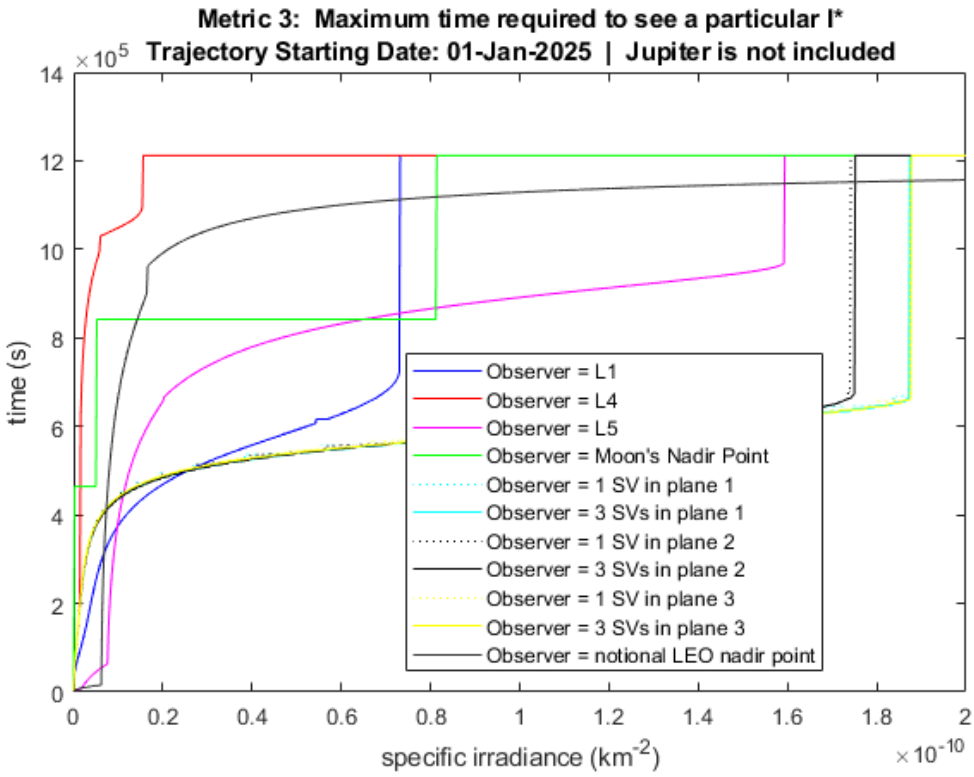

Figure 16. Metric 3 for a Sample Target Orbit

Metrics Aggregated

As Figure 13 makes clear, specific irradiance curves can vary greatly between similar target orbits, due to the very different orientation of the Sun compared to the Earth-Moon vector. The metrics similarly trend differently for slightly different orbits.

A comparison of Metric 1 for the original orbit and the equivalent orbit beginning 15 days later is shown in Figure 17. The juxtaposition clearly demonstrates that Metric 1 is very different when the starting time of the trajectory different by even a few days.

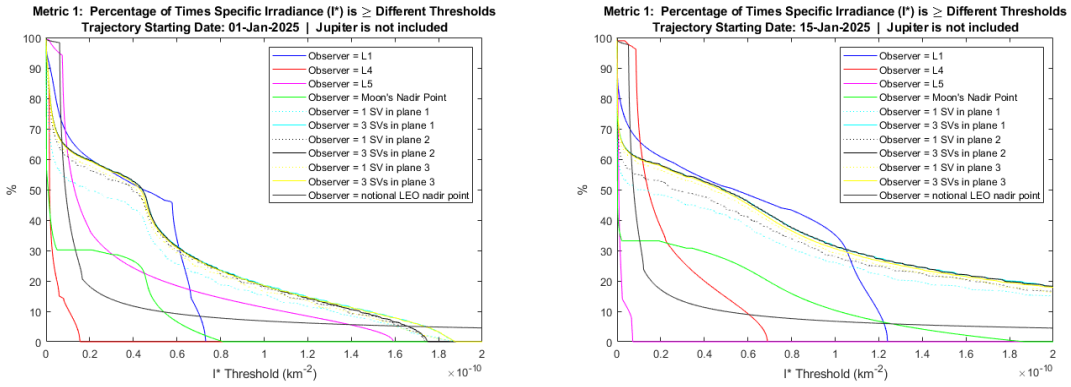

Figure 17. Comparison of Metric 1 for Two Target Orbits 15 Days Apart

A similar comparison of Metric 2 for the original orbit and the equivalent orbit beginning 15 days later is shown in Figure 18. Since Metric 2, when calculated for a single trajectory, is simply the specific irradiance curve scaled to a duration of 1000 dimensionless time units, the comparison in Figure 18 reflects the comparison of corresponding specific irradiance curves in Figure 13, and demonstrates that curves of Metric 2 also vary considerably when the trajectory starting time is varied even by a few days.

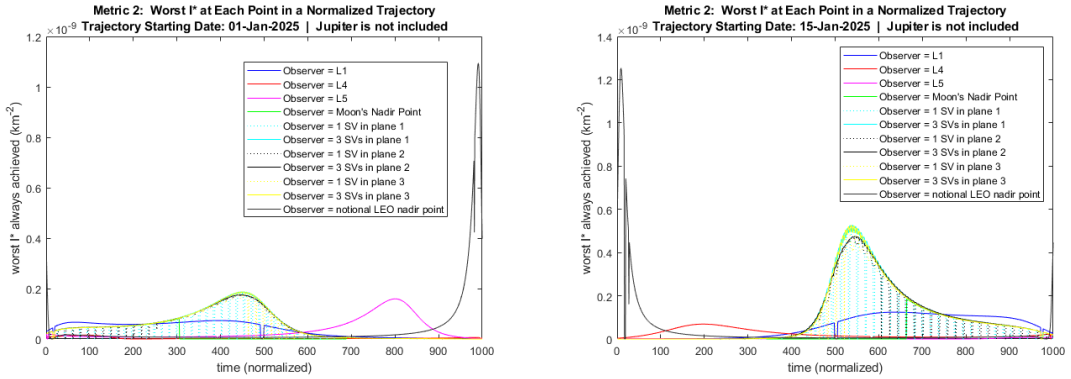

Figure 18. Comparison of Metric 2 for Two Target Orbits 15 Days Apart

Finally, a comparison of Metric 3 for the original orbit and the equivalent orbit beginning 15 days later is shown in Figure 19. This juxtaposition similarly shows that

curves of Metric 3 are significantly different when the trajectory starting time is varied even by a few days.

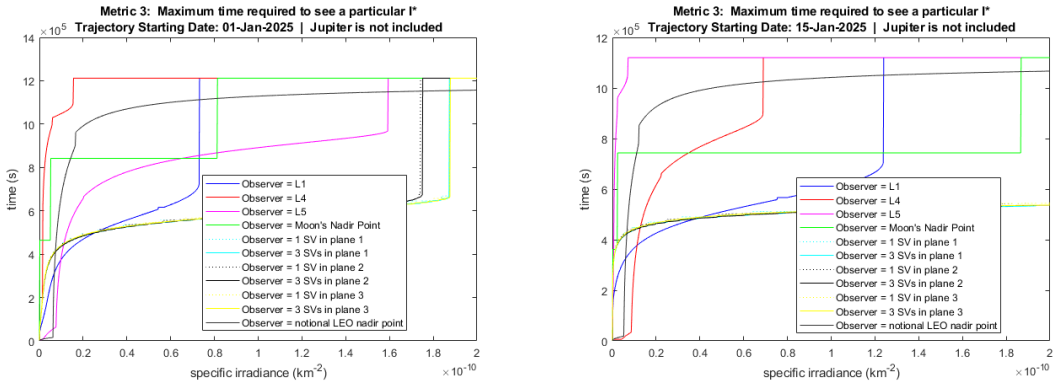

Figure 19. Comparison of Metric 3 for Two Target Orbits 15 Days Apart

The three metrics, aggregating specific irradiance data throughout all such trajectories across the decade of interest, should be a better indication of the observer stations' overall performance. Metric 1, *percentage of times specific irradiance is greater than or equal to different thresholds*, aggregated across the decade of interest for the 11 observer stations, is shown in Figure 20. The solid curves indicate the average values of the metric across all trajectories for the given values of specific irradiance threshold, and the dotted curves indicate the maximum and minimum values. In all three cases, the curves do not necessarily trace values of the metric for one particular trajectory, corresponding to a particular trajectory that always had the lowest, highest, or average values for the metric for every specific irradiance threshold; rather, each point represents the minimum, maximum, or average value reached. The solid curves appear smoother than any of the curves for a single trajectory in Figure 17, and the conglomeration of all observer stations in the same plot makes it possible to compare the overall effectiveness of different observer stations, with respect to Metric 1. For

example, the curve for L1 is always higher than the curve for the Moon's nadir point; this means that with respect to Metric 1, L1 is a *better* observer station than the Moon's nadir point. In other cases, one curve crosses another, so one observer station is not so definitively better than another. For example, the curve for L1 crosses the curve for a single satellite in low lunar orbit in a plane parallel to the Moon's orbit (Plane 1). To determine which observer station is better would depend on which specific irradiance thresholds are actually meaningful: If only values below the crossing point are meaningful, then L1 is more effective, but if only values above the crossing point are meaningful, then the single satellite in Plane 1 is better. To determine which values are meaningful would require insight about the sensor, and that is beyond the scope of this study. Instead, the effectiveness of two observer stations whose curves cross can be compared according to which curve is *usually* higher, and that can be determined based on average values.

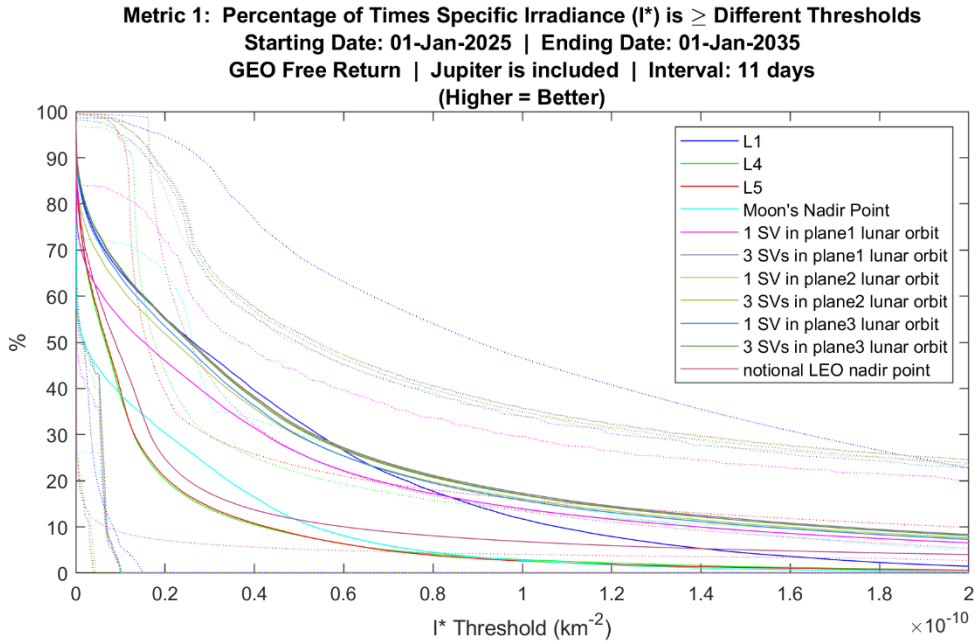

Figure 20. Metric 1 Aggregated Across a Decade

Metric 2, *worst specific irradiance at each point in a normalized trajectory*, aggregated across the decade of interest for the 11 observer stations, is shown in Figure 21. In this case, the curves are not smoother than those measuring Metric 2 for a single trajectory in Figure 18, but they do indicate something more meaningful than those curves for a single trajectory, since they reflect the worst values of specific irradiance measured across *many* trajectories.

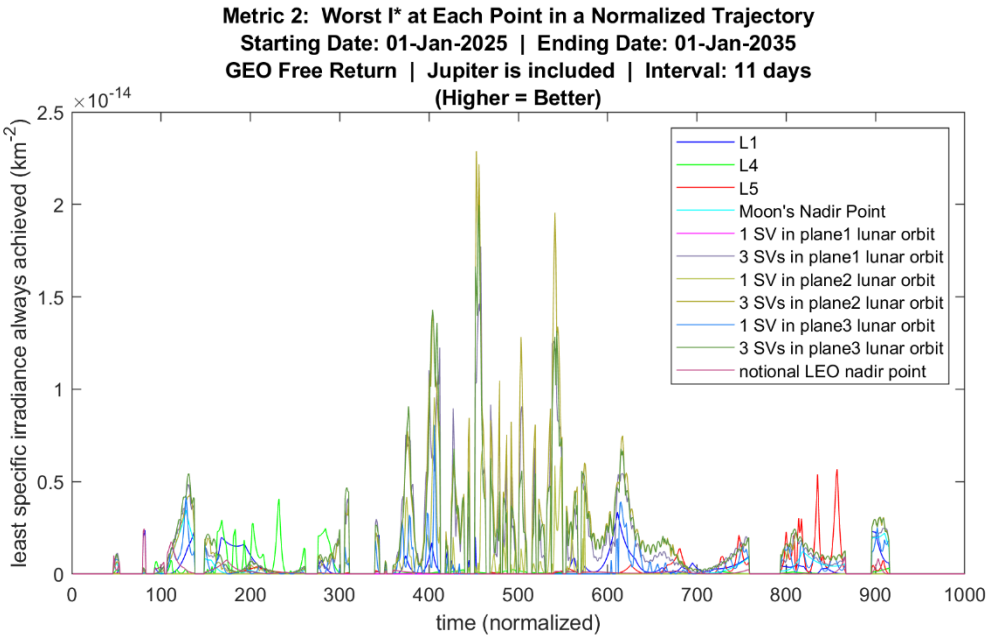

Figure 21. Metric 2 Aggregated Across a Decade

Metric 3, *maximum time required to see a particular irradiance*, aggregated across the decade of interest for the 11 observer stations, is shown in Figure 22. Here, solid curves again indicate average values, and dotted curves again indicate minimum and maximum values. Much like with Metric 1, Figure 22 indicates clearly that certain observer stations are more effective than others, *with respect to Metric 3*. For example, the curve for an observer at L1 is always lower than the curve for an observer at the Moon's nadir point; therefore, L1 is a better observer station than the Moon's nadir point

with respect to Metric 3, as it is with respect to Metric 1. Again, when one curve crosses another, insight about the sensor is needed in order to definitively determine which observer station is more effective; for example, the curves for an observer station at the Moon's nadir point crosses the curves for observer stations at L4 and L5. Of note, the curve for an observer at L1 does not cross the curve for a single satellite in Plane 1, as it did in Figure 20 for Metric 1. This means that although L1 is a definitively more effective observer station than a single satellite in Plane 1, *with respect to Metric 1*, it is not with respect to Metric 3; more to the point, the three metrics do not always rank observer stations identically.

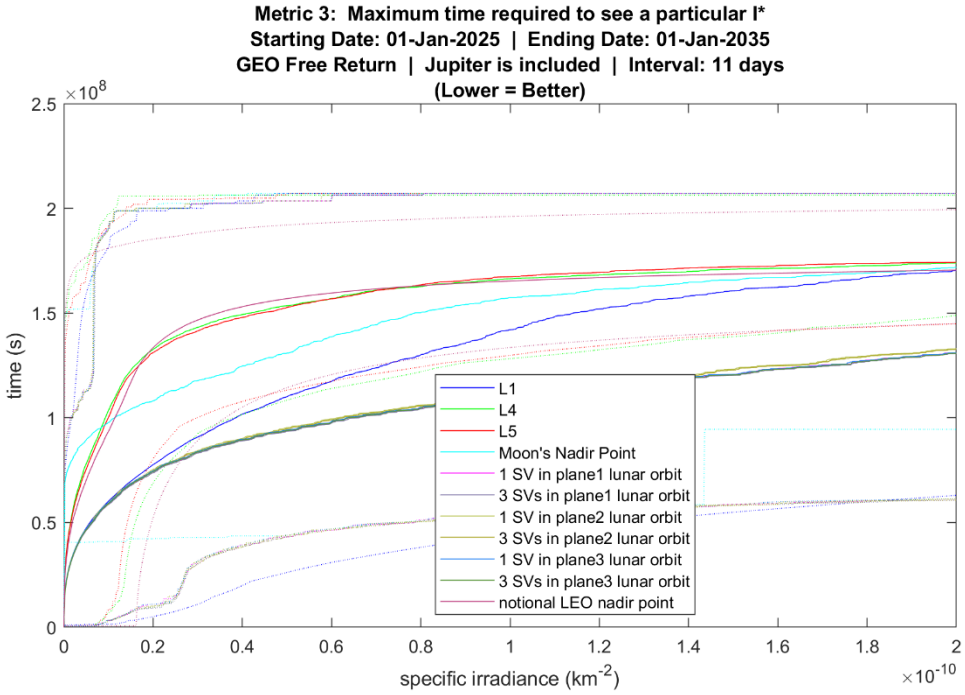

Figure 22. Metric 3 Aggregated Across a Decade

Results of Sensitivity Analysis

The sensitivity analysis consisted of repeating the simulation at regular intervals across the 2025-2035 decade with and without inclusion of the gravitational influence of

Jupiter in the dynamics model, and then repeating it with two different intervals. The results of the sensitivity analysis showed that the analysis overall was not especially sensitive either to other-body effects (beyond Sun, Earth, and Moon, and represented by Jupiter), or to the interval chosen, but the actual metrics had varying amounts of sensitivity to both.

The GEO free return was run with starting dates from January 1, 2025 through January 1, 2035, at intervals of 25 days, with and without inclusion of the gravitational influence of Jupiter in the dynamics model. The plots comparing Metric 1 for the same three observer stations with and without inclusion of Jupiter are shown side by side in Figure 23. While the solid "average" curves appear nearly identical, the shaded "minimum" and "maximum" curves appear to vary slightly. This demonstrates that while there may be even just two out of 146 runs in which Metric 1 is significantly altered by Jupiter's gravity, in aggregate, it is not.

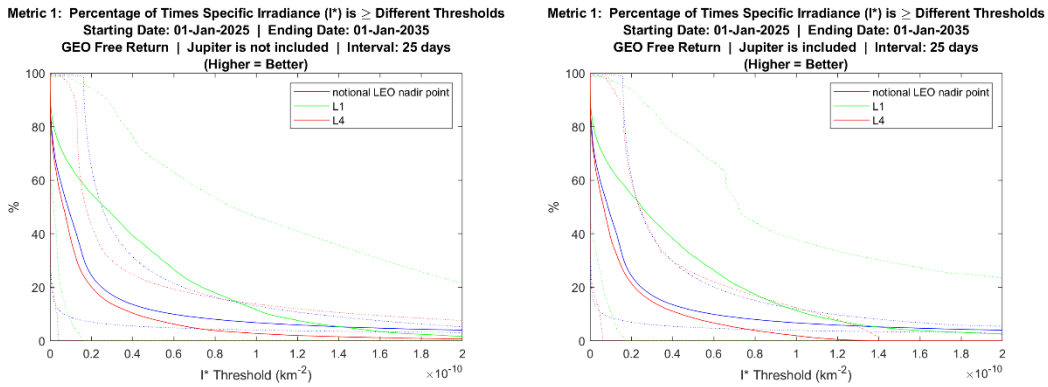

Figure 23. Comparison of Metric 1 With and Without Jupiter's Gravity

A similar comparison of Metric 2 is shown in Figure 24. In this case, the two plots look significantly different. This is likely due to the fact that Metric 2 always reflects only a single trajectory run at any given point, since it records the worst specific

irradiance experienced during any trajectory run at each normalized timestep. This may also indicate that comparing multiple similar orbits normalized into the same dimensionless duration may not be a very useful analytical tool. The results of this part of the sensitivity analysis demonstrate not only that Metric 2 is sensitive to the inclusion of other-body gravitational influences in the dynamics model, but that slight variations in the orbits result in significant variations of the metric; given that the ultimate goal of this study is to inform mission architecting and planning decisions where the full variety of cislunar orbits are of interest, Metric 2 may not be useful.

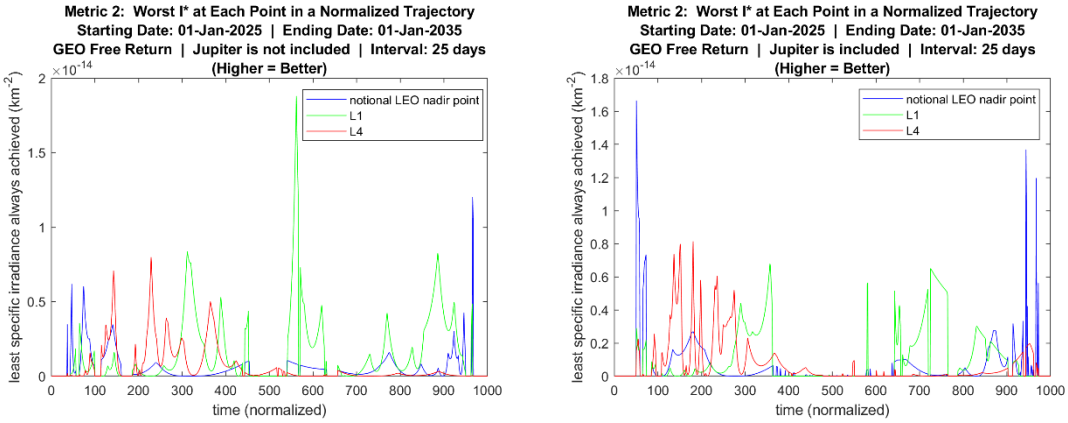

Figure 24. Comparison of Metric 2 With and Without Jupiter's Gravity

Finally, a similar comparison of Metric 3 is shown in Figure 25. Similar to the case of Metric 1, in the case of Metric 3, the solid "average" curves in the two plots look mostly similar, but the shaded "minimum" and "maximum" curves look different. The difference in the shaded curves is again likely due to the fact that they each reflect only a single trajectory run at any given point. The results of this part of the sensitivity analysis demonstrate that Metric 3 is only slightly sensitive to the inclusion of other-body gravitational influences in the dynamics model.

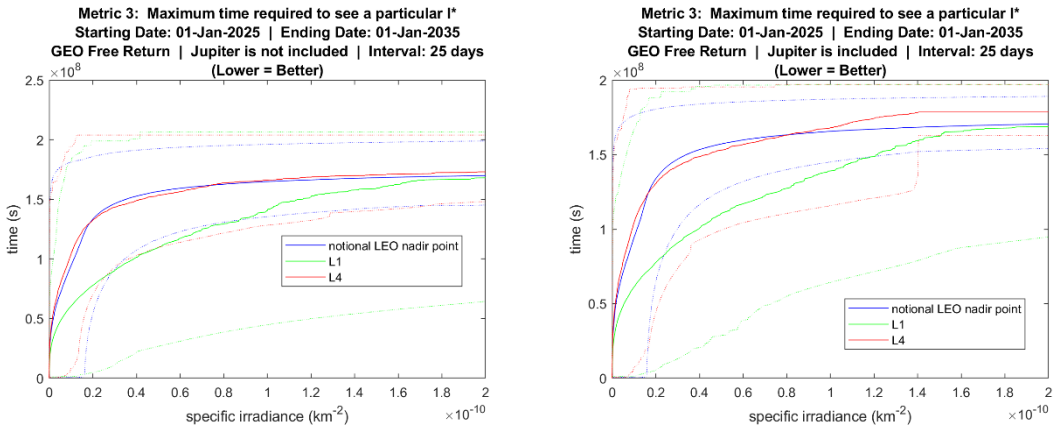

Figure 25. Comparison of Metric 3 With and Without Jupiter's Gravity

The rankings and scores (0-100) of all 11 observer stations are likewise shown side by side in Table 2 with and without inclusion of Jupiter's gravity in the dynamics model. The scores are used to distinguish a pair of observer stations that perform nearly equally from a pair whose performance gap is much greater. A score of 0 is assigned to the worst ranked observer station, and a score of 100 is assigned to the one that is highest ranked. All other scores are scaled linearly between 0 and 100 with respect to their average metric value. Where the ranking or score is the same with and without inclusion of Jupiter's gravity, both are highlighted in green. As the table shows, the rankings and scores are identical for all three metrics, so even though Metric 2 seemed to vary greatly, it ended up remaining essentially unchanged in aggregate; therefore, in aggregate, the analysis is not sensitive to other-body gravitational effects.

Table 2. Comparison of Metrics With and Without Jupiter's Gravity

Observer	Metric 1				Metric 2				Metric 3			
	no Jupiter		Jupiter		no Jupiter		Jupiter		no Jupiter		Jupiter	
	rank	score	rank	score	rank	score	rank	score	rank	score	rank	score
L1	6	75.4	6	75.4	4	24.3	4	24.3	7	48.5	7	48.5
L4	10	0.1	10	0.1	9	7.4	9	7.4	10	0.5	10	0.5
L5	11	0	11	0	7	8.4	7	8.4	11	0	11	0
Moon's Nadir	9	5.8	9	5.8	8	7.9	8	7.9	8	19.7	8	19.7
1 SV in Plane 1	7	73.2	7	73.2	11	0	11	0	3	99	3	99
3 SVs in Plane 1	1	100	1	100	3	75.3	3	75.3	1	100	1	100
1 SV in Plane 2	5	89.8	5	89.8	6	20.8	6	20.8	6	96.5	6	96.5
3 SVs in Plane 2	2	98.5	2	98.5	1	100	1	100	5	97.3	5	97.3
1 SV in Plane 3	4	90.8	4	90.8	5	22.2	5	22.2	4	98.8	4	98.8
3 SVs in Plane 3	3	97.8	3	97.8	2	94	2	94	2	99.4	2	99.4
Notional LEO Nadir	8	22.9	8	22.9	10	7.3	10	7.3	9	2.4	9	2.4

The GEO free return was run again without inclusion of the gravitational influence of Jupiter in the dynamics model, with starting dates from January 1, 2025 through January 1, 2035, but this time at intervals of 19 instead of 25 days. The plots comparing Metric 1 for the same three observer stations using the two different intervals are shown side by side in Figure 26. The "average" curves, and even the "minimum" and "maximum" curves appear essentially identical, so Metric 1 does not appear to be sensitive to the interval chosen.

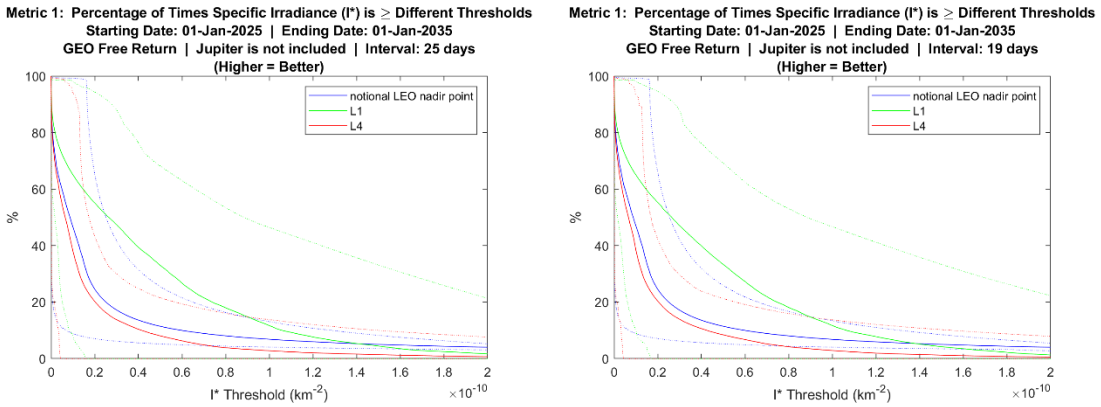

Figure 26. Comparison of Metric 1 Using Two Different Intervals

A similar comparison of Metric 2 is shown in Figure 27. In much the same way as with the comparison between inclusion and exclusion of Jupiter's gravity, the two plots look significantly different. This is again likely due to the fact that Metric 2 always reflects only a single trajectory run at any given point, and normalizing each trajectory into the same dimensionless time length may not be an analytically useful method. This result demonstrates not only that Metric 2 is sensitive to the interval used, but it also confirms that slight variations in the orbits result in significant variations of the metric, and it suggests that Metric 2 may not be useful for mission architecting and planning.

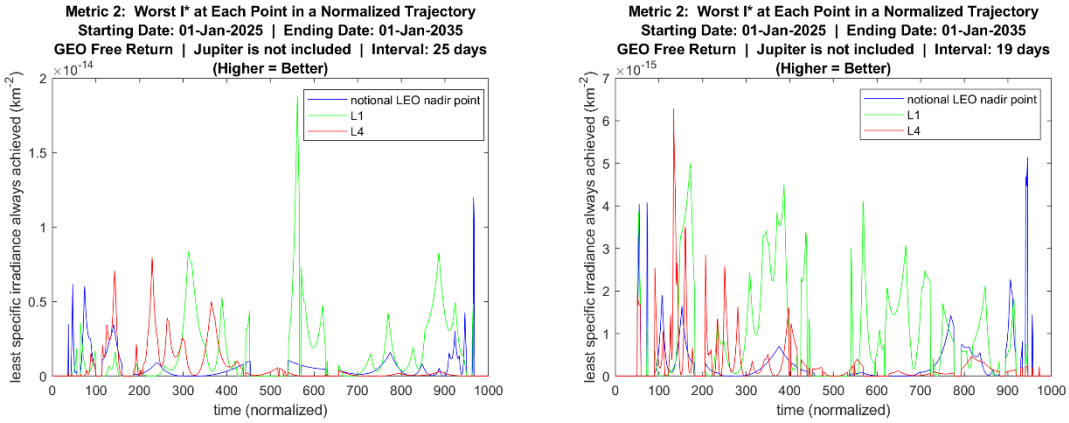

Figure 27. Comparison of Metric 2 Using Two Different Intervals

Finally, a similar comparison of Metric 3 is shown in Figure 28. All "average," "minimum," and "maximum" curves appear nearly identical for all three observers. This indicates that Metric 3 not sensitive to the interval used.

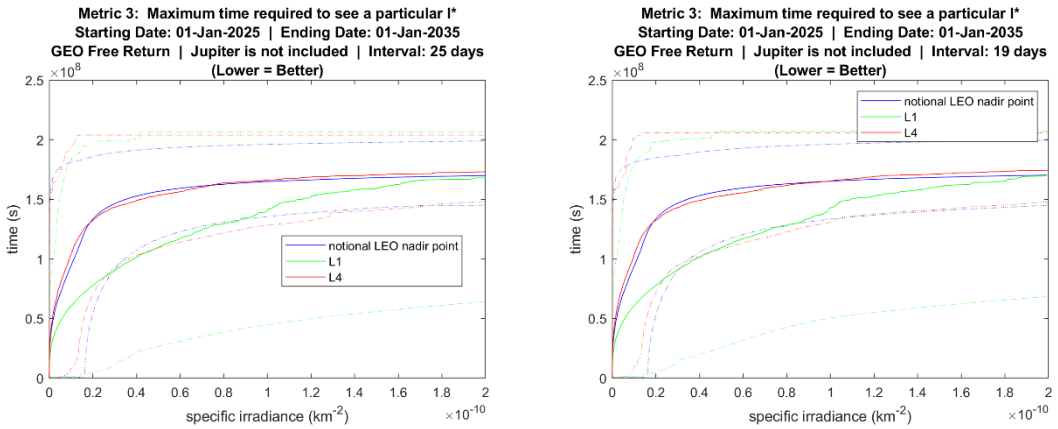

Figure 28. Comparison of Metric 3 Using Two Different Intervals

The rankings and scores of all 11 observer stations are again shown side by side in Table 3, again indicating identical rankings and scores in green. Table 3 confirms that Metric 1 and Metric 3, in aggregate, are relatively insensitive to the interval used, and Metric 2, in aggregate, is slightly more sensitive. That Table 3 shows much less green than Table 5 indicates the analysis in general is more sensitive to the interval chosen than to other-body gravitational effects.

Table 3. Comparison of Metrics Using Two Different Intervals

Observer	Metric 1				Metric 2				Metric 3			
	interval 19		interval 25		interval 19		interval 25		interval 19		interval 25	
	rank	score	rank	score	rank	score	rank	score	rank	score	rank	score
L1	6	75.4	6	75.8	4	24.3	4	28.9	7	48.5	7	48.6
L4	10	0.1	11	0	9	7.4	8	11.9	10	0.5	11	0
L5	11	0	10	0.5	7	8.4	9	10.1	11	0	10	0.3
Moon's Nadir	9	5.8	9	6.1	8	7.9	7	17	8	19.7	8	20.3
1 SV in Plane 1	7	73.2	7	73.2	11	0	11	0	3	99	3	99
3 SVs in Plane 1	1	100	1	100	3	75.3	3	82.9	1	100	1	100
1 SV in Plane 2	5	89.8	5	89.7	6	20.8	6	19	6	96.5	6	96.4
3 SVs in Plane 2	2	98.5	2	98.4	1	100	1	100	5	97.3	5	97.3
1 SV in Plane 3	4	90.8	4	90.8	5	22.2	5	23.8	4	98.8	4	98.8
3 SVs in Plane 3	3	97.8	3	97.9	2	94	2	92.8	2	99.4	2	99.4
Notional LEO Nadir	8	22.9	8	23.2	10	7.3	10	10	9	2.4	9	2.3

The relative insensitivity of Metric 1 and Metric 3 to inclusion or exclusion of Jupiter's gravity in the dynamics model, and to the interval used between trajectory runs, demonstrates that Metric 1 and Metric 3 are reliable, that the conclusions based on them are representative of reality, and that they may be useful for the purpose of mission architecting and planning. Metric 1 and Metric 3 have been shown to both effectively aggregate information about the performance of an observer station in a way that is consistent across many trajectories, and that is not affected by small perturbations to the trajectories. While Metric 2 proved more sensitive to the two variables tested, and may therefore not be as useful for mission architecting and planning, it may still have utility in assessing a specific observer's performance against a specific target. This can be of great value in operations.

General Results

Since the sensitivity analysis demonstrated that Metric 1 and Metric 3 were suitable for comparing and ranking observer stations generally, but Metric 2 was less so, only the results with respect to Metric 1 and Metric 3 are reported here. The sensitivity analysis showed minimal sensitivity of Metric 1 and Metric 3 to the inclusion of Jupiter's gravity in the dynamics model, and to a change in the interval used between trajectory runs, but since that sensitivity was not zero, the results reported here are from a run that used a more precise choice of each of the variables tested. That run included Jupiter's gravity in the dynamics model, and used an interval of 11 days instead of 19 or 25. The curves for Metric 1 and Metric 3 of all 11 observer stations are combined in Figure 29 and Figure 30, respectively.

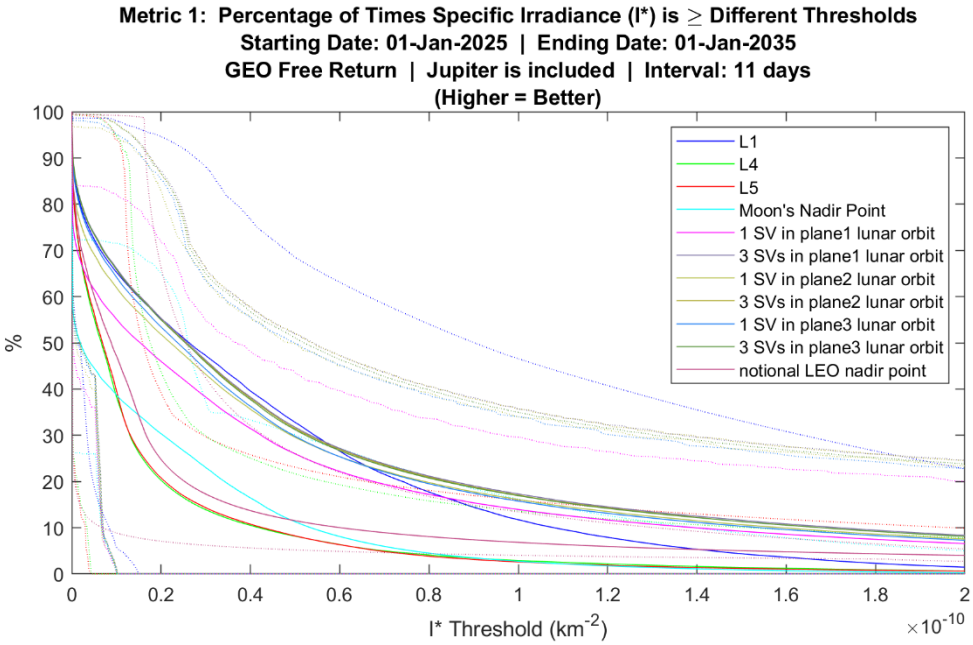

Figure 29. Metric 1 for All 11 Observer Stations

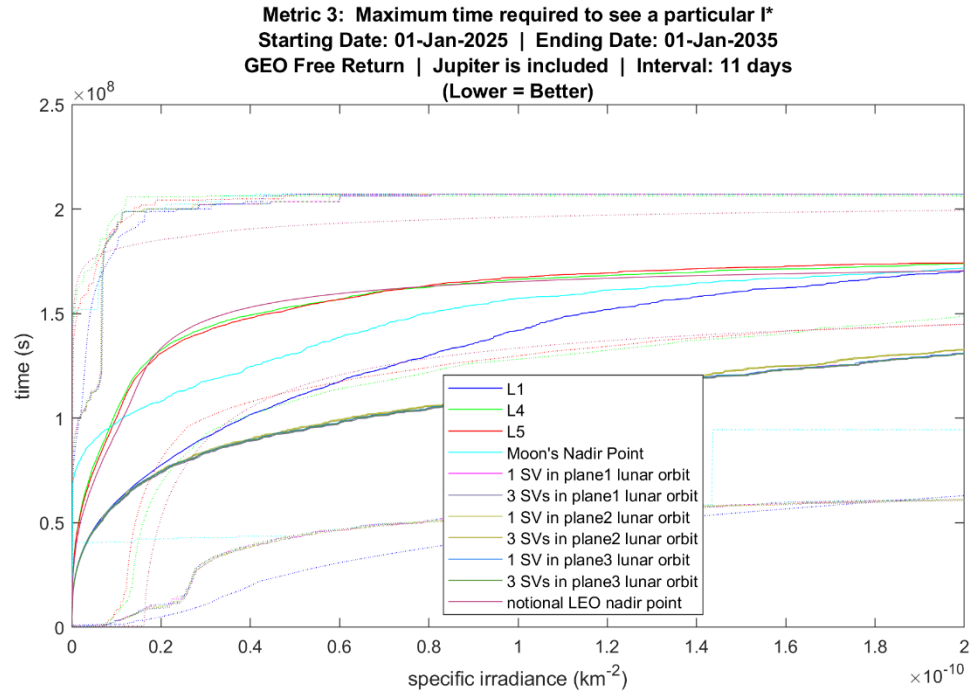

Figure 30. Metric 3 for All 11 Observer Stations

Metric 1 and Metric 3 for the "stationary" observers alone are isolated in Figure 31 and Figure 32, respectively. Those plots make clear whenever two curves cross that one observer is not necessarily *always* better than another, but one can be said to be *generally* better than another.

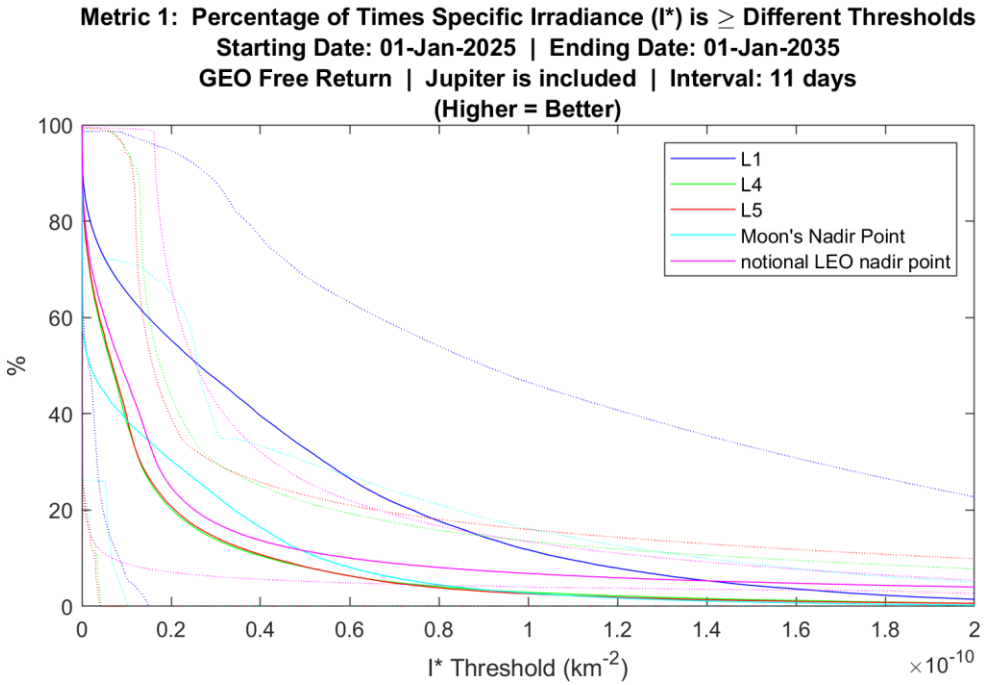

Figure 31. Metric 1 for All Observer Stations Stationary in ECMF

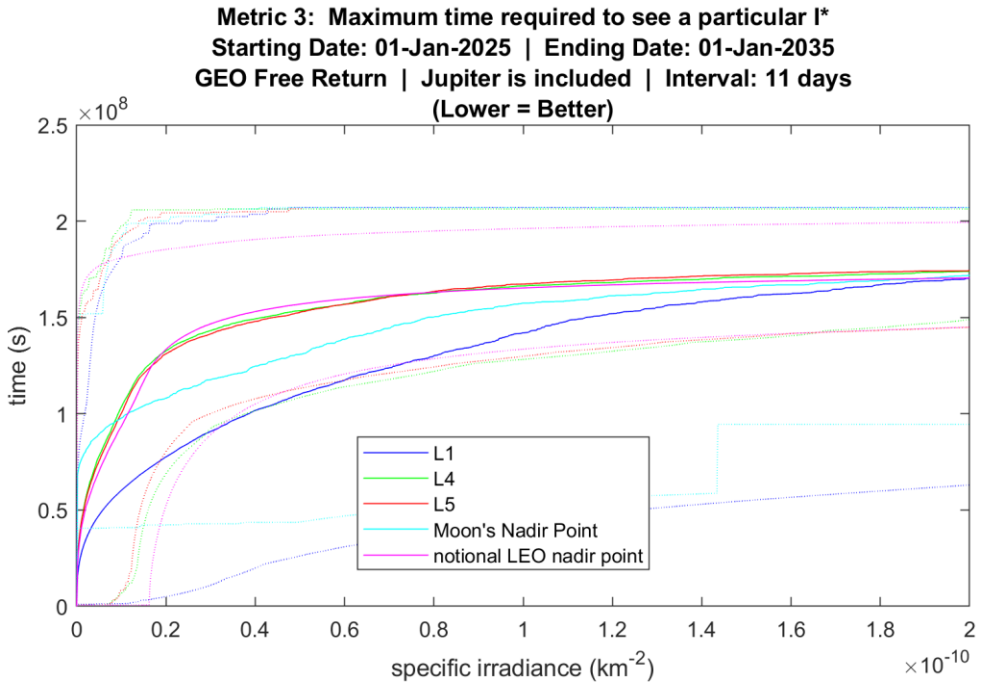

Figure 32. Metric 3 for All Observer Stations Stationary in ECMF

A ranking of the 11 observer stations and 93 meaningful combinations of observer stations, with scores, is shown in Table 5 in Appendix B. A sample excluding the combinations is shown in Table 4. The high ranks and scores of zero for Metric 2 indicate that combinations of observer stations resulted in much higher values of that metric. It measures the *worst* specific irradiance seen at each point, and this can be zero when any single observer on its own is blocked from viewing the target, but combinations of observers are much less susceptible to that effect, so this is not surprising.

Table 4. Metrics Ranked and Scored for All Observer Stations

Observer or Combination of Observers	Metric 1		Metric 2		Metric 3	
	Rank	Score	Rank	Score	Rank	Score
L1	92	44.5	97	0	96	33.2
L4	103	0.1	102	0	103	0.3
L5	104	0	100	0	104	0
Moon's Nadir Point	102	3.2	101	0	101	13.4
1 SV in plane1 lunar orbit	94	42.8	104	0	81	67.2
3 SVs in plane1 lunar orbit	81	58.5	92	0	74	67.9
1 SV in plane2 lunar orbit	89	52.6	98	0	88	65.5
3 SVs in plane2 lunar orbit	83	57.6	89	0	86	66
1 SV in plane3 lunar orbit	88	53.1	96	0	83	67.1
3 SVs in plane3 lunar orbit	85	57.3	90	0	79	67.5
notional LEO nadir point	101	13.7	103	0	102	1.5

Investigative Questions Answered

This study has answered all three investigative questions:

1) *What general category of orbits would put an observer satellite in the position of observing objects in cislunar space with the greatest brightness of reflected sunlight?* The answer is presented in the form of a ranked and scored list of observers and combinations of observers in Table 5 in Appendix B. Among single observer stations, constellations in low circular lunar orbit performed the best, and due to the tendency for their view of a target satellite to be blocked by the Moon, single satellites in low circular lunar orbit performed slightly worse. L1 performed better than L4 or L5, likely because it was closer to the target satellite during the extended part of that satellite's orbit when it is close to the Moon. Even despite its tendency to be blocked by the Moon, a point on the lunar surface at the nadir point performed better than L4 or L5, but not as well as L1. A notional point in LEO on the Moon-facing side of Earth performed better than the lunar surface nadir point, L4, or L5.

2) *How would the suitability of combinations of those categories of orbits compare?*

   The answer is presented in the form of a ranked and scored list of observers and combinations of observers in Table 5, which includes both single observer stations and combinations of observer stations. In general, combinations are more effective than individual stations, as would be expected. Combinations of stations very far apart are especially beneficial. For observers in low circular lunar orbit, combinations of multiple such stations produce noticeable improvements, likely because they negate the limitation of observation due to eclipsing by the Moon: When the Moon blocks one satellite's view, another well-placed satellite is not similarly blocked.

3) *What metrics can be used to reliably compare the suitability of different such categories of orbits?*

   Metric 1 and Metric 3 have been shown to serve this purpose well, and they were used to answer the first two investigative questions. Metric 2 has been shown to be less effective for this purpose, although it may be useful for assessing a specific observer's performance against a specific target, which could be of great value in operations.

Summary

Since the sensitivity analysis showed that Metric 2 was not suitable for comparing observer stations for the purpose of general cislunar Space Domain Awareness mission architecting, only Metric 1 and Metric 3 are used here to rank those observer stations and combinations of observer stations. The final results, counting the 11 representative

observer stations and several meaningful combinations of observer stations, are shown in Table 5 in Appendix B. A score is also included for each, from zero to 100. That score normalizes the values of each metric so that the observer or combination of observers with the highest value is assigned a score of 100, the one with the lowest value is assigned a score of zero, and all others are scaled linearly. The purpose of the scores is to show how much better one observer or combination of observers is than another, and also when two are actually equal, even if the sorting algorithm has artificially ranked one above the other.

V. Conclusions and Recommendations

Chapter Overview

This chapter summarizes the conclusions of this research, expounds on its significance and utility to mission planning, suggests how it may be used to advance the state of cislunar Space Domain Awareness, and finally identifies several areas of worthwhile follow-up research.

Conclusions of Research

The most significant and surprising conclusion from this analysis is that a single observer at L4 or L5 would be *less* effective at observing satellites in circumlunar free returns than a constellation of sensors in LEO, based on the chosen metrics. The full set of conclusions concerning how the different observer stations and meaningful combinations thereof compare can be seen in Table 5 in Appendix B. Several useful insights can be gleaned from that ranking and the associated scores:

- As mentioned, a single observer at L4 or L5 would be less effective at observing satellites in circumlunar free returns than a constellation of sensors in LEO, but when both L4 and L5 are combined, the result is significantly better than for a constellation in LEO. When L4 or L5 is combined with L1, the result is significantly better still.
- L4 or L5 combined with L1 will be more effective than any combination of observers in low circular lunar orbit or on the lunar surface near the nadir point.
- An observer on the lunar surface near the Moon's nadir point will add negligible value if there is already an observer near the Earth-Moon L1 point, but the reverse is not true: L1 is a much more effective observer station than the nadir point on the lunar surface, likely because the Moon itself blocks so much of the latter's view. This is true of the approximate L1 point itself, but subsequent research would be required to determine if the same is true of quasi-periodic orbits in the vicinity of L1, to include Halo orbits.

There is no practical limit to the number of similar insights this analysis could provide, since it offers the ability to record any other combinations of observers not listed here.

Significance of Research

To the author's knowledge, this study is the first to investigate the effectiveness of several general categories of orbits for use in stationing satellites that would observe other objects in cislunar space for the purpose of achieving Space Domain Awareness in that domain. It can inform mission planning for this vital emerging mission, and it provides a stepping stone toward further research to determine optimal stations for such

satellites, so they could most effectively detect and track objects in many varieties of operationally relevant cislunar orbits.

Recommendations for Action

Further study would be required before formal mission planning, but the results of this study should inform the general architecting of a program meant to achieve cislunar Space Domain Awareness. Based on these results, planners of such a program should consider combining data from sensors in LEO with that from sensors in low circular lunar orbit.

Recommendations for Future Research

This research was meant as an initial investigation into which orbital stations would generally perform well and which would perform poorly for the purpose of cislunar Space Domain Awareness. It addressed specific categories of observer stations and specific target trajectories using specific metrics. A logical next step would be to expand the set of observer stations, target trajectories, and metrics, in order to determine if the same results would emerge.

Many of the fourteen observer stations addressed in this research were meant to represent observer satellites in broad classes of orbits, but there are no limitations in the MATLAB code that would prevent them from being replaced with realistic orbits. In particular, stationary points in the ECMF frame approximating solutions to the CR3BP that manifest as stationary points in the synodic frame, particularly the L1, L4, and L5 Lagrangian points, could be replaced with realistic orbits in the vicinity of those points. Likewise, the notional point at 800 km altitude above Earth, permanently on the Moon-

facing side, could be replaced by one or a collection of real LEO orbits representing a realistic constellation of observer satellites in LEO. The present investigation assumed the Earth and Moon were uniform spheres, but to accurately model a constellation of satellites in LEO would require the inclusion of the Earth's asphericity and variable gravitational field. In addition to refining the observer orbits, a subsequent investigation could also add observers in other novel orbits, such as a constellation in highly eccentric Earth orbit arranged such that at least one satellite would always appear to be in a translunar free return trajectory.

This research only addressed one class of target trajectories, coplanar circumlunar free returns originating from GEO. The results may be representative of other cislunar trajectories, but this research made no such determination, and makes no such claim. It would, however, be relatively straightforward to repeat it for other types of translunar free returns, as well as other realistic cislunar orbits, such as those that orbit the L1, L4, and L5 Earth-Moon Lagrangian Points. Rather than repeat exactly the same free return trajectory throughout the decade of interest, the model used in this research produced a slightly different trajectory each time, demonstrating a sensitivity to initial conditions, and producing no consistency in the perilune distance. This was taken as an advantage, producing a representative family of trajectories rather than a single one, but greater precision in the results could be achieved by repeating exactly the same trajectory each time throughout a decade, and then repeating the entire analysis for many other specific trajectories. To do this would simply require a function that finds the starting conditions necessary for the target satellite to complete a circumlunar free return with a specified perilune distance. When applied to a free return originating from LEO, the analysis

failed because those orbits were much more sensitive to the initial conditions, and the algorithm used to optimize the initial conditions was not robust enough. Improving that algorithm and applying the analysis to other classes of free returns would be a useful next step.

The metrics could likewise be improved upon, not by adding or modifying metrics, but by framing them in terms of realistic mission requirements. In particular, Metric 1, *percentage of times specific irradiance is greater than or equal to different thresholds*, measures how often the specific irradiance is above different thresholds, without consideration of which thresholds are meaningful. A more meaningful version of Metric 1, for use in actual mission architecting and planning, would measure how often the actual irradiance is above the threshold of detection for a sensor that may be used in an actual mission, given the realistic properties of a target satellite. Likewise, a plot of Metric 2, *worst specific irradiance at each point in a normalized trajectory*, may engender greater insight if those minimum thresholds of detection were included as horizontal lines on the plot. Metric 3, *maximum time required to see a particular irradiance*, might also be reported in such a way as to emphasize the *particular* irradiance measures associated with one or several actual sensors under consideration for a mission, coupled with actual representative target satellites.

This study ignored the theoretical precision of an orbit determination, which would depend on geometry through a different relation that would irradiance. A future study should take into account precision of orbit determination in comparing observer schemes, especially in judging favorably combinations of observer stations that give observer views of objects from very different angles.

Summary

This research succeeded in determining which of fourteen chosen observer stations was best for observing satellites in circumlunar free return trajectories, although that result was different depending on how "best" was defined. In general, it demonstrated that some, but not all, observer stations studied could achieve better performance than a constellation of ground-based and/or LEO-based sensors. The conclusions narrowly apply to targets in circumlunar free returns, so further study utilizing the tools developed for this study would be warranted, and would further contribute to the design of a cislunar Space Domain Awareness mission.

Appendix A: Derivation of Equation for Location of Earth-Moon L1

Expressed along the Earth-Moon axis, Newton's law of universal gravitation and Newton's second law applied to a satellite become 1-dimensional, with the origin at Earth, and the Moon in the positive direction.

$$F_{Gravity,Earth} - F_{Gravity,Moon} = M_{SV}a$$

Combined with the expression for centripetal acceleration, $\frac{V^2}{r}$, this can be rewritten in terms of the orbital period:

$$\frac{GM_{Earth}M_{SV}}{(r_{EarthMoon} - D_{L1})^2} - \frac{GM_{Moon}M_{SV}}{{D_{L1}}^2} = M_{SV}\frac{{V_{SV}}^2}{r_{BarycenterMoon} - D_{L1}}$$

$$\frac{GM_{Earth}}{(r_{EarthMoon} - D_{L1})^2} - \frac{GM_{Moon}}{{D_{L1}}^2} = \frac{{V_{SV}}^2}{r_{BarycenterMoon} - D_{L1}}$$

$$\frac{\mu_{Earth}}{(r_{EarthMoon} - D_{L1})^2} - \frac{\mu_{Moon}}{{D_{L1}}^2} = \frac{\left(\frac{2\pi(r_{BarycenterMoon} - D_{L1})}{T_{Moon}}\right)^2}{r_{BarycenterMoon} - D_{L1}}$$

$$\frac{\mu_{Earth}}{(r_{EarthMoon} - D_{L1})^2} - \frac{\mu_{Moon}}{{D_{L1}}^2} = \frac{\left(2\pi(r_{BarycenterMoon} - D_{L1})\right)^2}{(r_{BarycenterMoon} - D_{L1}){T_{Moon}}^2} \quad (11)$$

The period of the Moon's orbit, T_{Moon}, is found by applying Newton's law of universal gravitation and Newton's second law to the Earth-Moon orbit itself:

$$\frac{GM_{Earth}M_{Moon}}{{r_{EarthMoon}}^2} = M_{Moon}\frac{{V_{Moon}}^2}{r_{BarycenterMoon}}$$

$$\frac{\mu_{Earth}}{{r_{EarthMoon}}^2} = \frac{{V_{Moon}}^2}{r_{BarycenterMoon}} = \frac{\left(\frac{2\pi r_{BarycenterMoon}}{T_{Moon}}\right)^2}{r_{BarycenterMoon}} = \left(\frac{2\pi}{T_{Moon}}\right)^2 r_{BarycenterMoon}$$

$${T_{Moon}}^2 = \frac{(2\pi r_{EarthMoon})^2 r_{BarycenterMoon}}{\mu_{Earth}}$$

The ${T_{Moon}}^2$ term can then be substituted into Equation (11).

$$\frac{\mu_{Earth}}{(r_{EarthMoon} - D_{L1})^2} - \frac{\mu_{Moon}}{{D_{L1}}^2}$$

$$= \frac{\left(2\pi\left(r_{BarycenterMoon} - D_{L1}\right)\right)^2}{\left(r_{BarycenterMoon} - D_{L1}\right)\frac{(2\pi r_{EarthMoon})^2 r_{BarycenterMoon}}{\mu_{Earth}}}$$

$$\frac{\mu_{Earth}}{(r_{EarthMoon} - D_{L1})^2} - \frac{\mu_{Moon}}{{D_{L1}}^2} = \frac{\mu_{Earth}\left(r_{BarycenterMoon} - D_{L1}\right)}{{r_{EarthMoon}}^2 r_{BarycenterMoon}} \quad (12)$$

The distance from Earth to the Earth-Moon barycenter can be found like any other center of mass, and the Earth-Moon distance is simply the sum of that and the distance from the Earth-Moon barycenter to the Moon.

$$r_{EarthBarycenter} = r_{EarthMoon}\frac{M_{Moon}}{M_{Earth} + M_{Moon}} = r_{EarthMoon} - r_{BarycenterMoon}$$

$$r_{BarycenterMoon} = r_{EarthMoon} - r_{EarthMoon}\frac{M_{Moon}}{M_{Earth} + M_{Moon}}$$

$$r_{BarycenterMoon} = r_{EarthMoon}\left(1 - \frac{\mu_{Moon}}{\mu_{Earth} + \mu_{Moon}}\right)$$

This expression for $r_{BarycenterMoon}$ can then be substituted into Equation (12).

$$\frac{\mu_{Earth}}{(r_{EarthMoon} - D_{L1})^2} - \frac{\mu_{Moon}}{{D_{L1}}^2} = \frac{\mu_{Earth}\left(r_{EarthMoon}\left(1 - \frac{\mu_{Moon}}{\mu_{Earth} + \mu_{Moon}}\right) - D_{L1}\right)}{{r_{EarthMoon}}^2 r_{EarthMoon}\left(1 - \frac{\mu_{Moon}}{\mu_{Earth} + \mu_{Moon}}\right)}$$

$$\frac{\mu_{Earth}}{(r_{EarthMoon} - D_{L1})^2} = \frac{\mu_{Moon}}{{D_{L1}}^2} + \frac{\mu_{Earth}\left(r_{EarthMoon}\left(\frac{\mu_{Earth} + \mu_{Moon}}{\mu_{Earth} + \mu_{Moon}} - \frac{\mu_{Moon}}{\mu_{Earth} + \mu_{Moon}}\right) - D_{L1}\right)}{{r_{EarthMoon}}^3\left(\frac{\mu_{Earth} + \mu_{Moon}}{\mu_{Earth} + \mu_{Moon}} - \frac{\mu_{Moon}}{\mu_{Earth} + \mu_{Moon}}\right)}$$

$$\frac{\mu_{Earth}}{(r_{EarthMoon} - D_{L1})^2} = \frac{\mu_{Moon}}{{D_{L1}}^2} + \frac{\mu_{Earth}\left(r_{EarthMoon}\left(\frac{\mu_{Earth}}{\mu_{Earth} + \mu_{Moon}}\right) - D_{L1}\right)}{{r_{EarthMoon}}^3\left(\frac{\mu_{Earth}}{\mu_{Earth} + \mu_{Moon}}\right)}$$

$$\frac{\mu_{Earth}}{(r_{EarthMoon} - D_{L1})^2} = \frac{\mu_{Moon}}{{D_{L1}}^2} + \left(\frac{\mu_{Earth}}{\mu_{Earth} + \mu_{Moon}} r_{EarthMoon} - D_{L1}\right)\frac{\mu_{Earth} + \mu_{Moon}}{{r_{EarthMoon}}^3} \quad (2)$$

This is the equation that can be solved numerically for D_{L1} in order to locate L1.

Appendix B: Full Table of Results

Table 5. Metrics Ranked and Scored for All Observers and Combinations

Observer or Combination of Observers	Metric 1		Metric 2		Metric 3	
	Rank	Score	Rank	Score	Rank	Score
L1	92	44.5	97	0	96	33.2
L4	103	0.1	102	0	103	0.3
L5	104	0	100	0	104	0
Moon's Nadir Point	102	3.2	101	0	101	13.4
L1, L4	78	61	58	36	90	50.1
L1, L5	79	60.6	38	46.2	91	49.8
L4, L5	100	23.6	64	27.6	98	23.6
L1, L4, L5	39	76.8	22	84.3	84	66.6
L1, nadir	91	46.7	86	0.1	93	38.9
L4, nadir	98	24.4	63	29.5	94	33.9
L5, nadir	99	24	61	33.2	95	33.2
L4, L5, nadir	93	43.4	25	69.2	89	52.8
L1, L4, L5, nadir	38	78.7	13	91.1	63	72
1 SV in plane1 lunar orbit	94	42.8	104	0	81	67.2
3 SVs in plane1 lunar orbit	81	58.5	92	0	74	67.9
1 SV in plane2 lunar orbit	89	52.6	98	0	88	65.5
3 SVs in plane2 lunar orbit	83	57.6	89	0	86	66
1 SV in plane3 lunar orbit	88	53.1	96	0	83	67.1
3 SVs in plane3 lunar orbit	85	57.3	90	0	79	67.5
L1, 1 SV in plane1 lunar orbit	75	63.2	87	0.1	69	69.5
L1, 3 SVs in plane1 lunar orbit	62	68.4	72	0.3	64	70
L1, 1 SV in plane2 lunar orbit	69	66.1	81	0.2	77	67.8
L1, 3 SVs in plane2 lunar orbit	66	67.6	76	0.3	72	68.2
L1, 1 SV in plane3 lunar orbit	73	65.2	80	0.2	71	69.4
L1, 3 SVs in plane3 lunar orbit	65	67.8	74	0.3	66	69.7
L4, 1 SV in plane1 lunar orbit	76	61.8	82	0.2	52	82.1
L4, 3 SVs in plane1 lunar orbit	41	75.7	48	38	46	82.7
L4, 1 SV in plane2 lunar orbit	59	70.5	70	6.3	62	80.5
L4, 3 SVs in plane2 lunar orbit	45	74.9	54	37.7	60	81.1
L4, 1 SV in plane3 lunar orbit	57	70.6	57	36.9	54	82
L4, 3 SVs in plane3 lunar orbit	47	74.5	52	37.8	50	82.4
L5, 1 SV in plane1 lunar orbit	77	61.5	85	0.1	42	83.1
L5, 3 SVs in plane1 lunar orbit	43	75.3	32	47.4	34	83.7
L5, 1 SV in plane2 lunar orbit	61	70.1	71	2.5	58	81.4
L5, 3 SVs in plane2 lunar orbit	49	74.5	37	46.8	56	82
L5, 1 SV in plane3 lunar orbit	60	70.2	41	44.1	44	82.9

L5, 3 SVs in plane3 lunar orbit	51	74.1	35	47.2	39	83.3
Moon's nadir, 1 SV in plane1 lunar orbit	90	48	99	0	80	67.2
Moon's nadir, 3 SVs in plane1 lunar orbit	80	58.5	93	0	75	67.9
Moon's nadir, 1 SV in plane2 lunar orbit	86	55.5	94	0	87	65.5
Moon's nadir, 3 SVs in plane2 lunar orbit	82	57.6	88	0	85	66
Moon's nadir, 1 SV in plane3 lunar orbit	87	53.5	95	0	82	67.1
Moon's nadir, 3 SVs in plane3 lunar orbit	84	57.4	91	0	78	67.5
L1, L4, 1 SV in plane1 lunar orbit	36	79.3	47	40.7	32	84
L1, L4, 3 SVs in plane1 lunar orbit	24	84.5	42	43.6	29	84.5
L1, L4, 1 SV in plane2 lunar orbit	31	82.2	46	42.8	48	82.4
L1, L4, 3 SVs in plane2 lunar orbit	27	83.7	44	43.3	45	82.8
L1, L4, 1 SV in plane3 lunar orbit	33	81.3	45	43	33	83.9
L1, L4, 3 SVs in plane3 lunar orbit	26	83.8	43	43.5	30	84.3
L1, L5, 1 SV in plane1 lunar orbit	37	79	31	50.6	27	84.9
L1, L5, 3 SVs in plane1 lunar orbit	25	84.1	26	55.5	25	85.4
L1, L5, 1 SV in plane2 lunar orbit	32	81.8	29	54.3	40	83.2
L1, L5, 3 SVs in plane2 lunar orbit	29	83.3	28	54.9	36	83.7
L1, L5, 1 SV in plane3 lunar orbit	34	80.9	30	54.2	28	84.8
L1, L5, 3 SVs in plane3 lunar orbit	28	83.4	27	55.4	26	85.1
L4, L5, 1 SV in plane1 lunar orbit	35	79.5	60	33.8	16	98.2
L4, L5, 3 SVs in plane1 lunar orbit	14	92.3	14	88.1	9	98.8
L4, L5, 1 SV in plane2 lunar orbit	22	87.6	39	45.9	24	96.7
L4, L5, 3 SVs in plane2 lunar orbit	16	91.4	19	87.2	22	97.2
L4, L5, 1 SV in plane3 lunar orbit	23	87.4	21	85.8	18	98.1
L4, L5, 3 SVs in plane3 lunar orbit	18	91.1	17	87.7	12	98.5
L1, L4, L5, 1 SV in plane1 lunar orbit	12	94.9	12	92.9	6	99.5
L1, L4, L5, 3 SVs in plane1 lunar orbit	1	100	1	100	1	100
L1, L4, L5, 1 SV in plane2 lunar orbit	8	97.8	10	98.1	20	98
L1, L4, L5, 3 SVs in plane2 lunar orbit	5	99.2	5	99.1	13	98.4
L1, L4, L5, 1 SV in plane3 lunar orbit	10	96.9	9	98.5	8	99.4
L1, L4, L5, 3 SVs in plane3 lunar orbit	4	99.4	3	99.9	3	99.8
L1, Moon's nadir, 1 SV in plane1	74	63.6	83	0.1	68	69.5
L1, Moon's nadir, 3 SVs in plane1	63	68.4	73	0.3	65	70
L1, Moon's nadir, 1 SV in plane2	68	66.3	78	0.2	76	67.8
L1, Moon's nadir, 3 SVs in plane2	67	67.6	77	0.3	73	68.2
L1, Moon's nadir, 1 SV in plane3	72	65.3	79	0.2	70	69.4
L1, Moon's nadir, 3 SVs in plane3	64	67.8	75	0.3	67	69.7
L4, Moon's nadir, 1 SV in plane1	70	65.9	62	30	51	82.1
L4, Moon's nadir, 3 SVs in plane1	40	75.7	49	38	47	82.7
L4, Moon's nadir, 1 SV in plane2	53	72.8	55	37.1	61	80.6
L4, Moon's nadir, 3 SVs in plane2	44	74.9	53	37.7	59	81.1
L4, Moon's nadir, 1 SV in plane3	56	71	56	37	53	82

L4, Moon's nadir, 3 SVs in plane3	46	74.6	51	37.8	49	82.4
L5, Moon's nadir, 1 SV in plane1	71	65.5	59	34.3	41	83.1
L5, Moon's nadir, 3 SVs in plane1	42	75.3	33	47.4	35	83.7
L5, Moon's nadir, 1 SV in plane2	54	72.5	50	37.9	57	81.5
L5, Moon's nadir, 3 SVs in plane2	48	74.5	36	46.8	55	82
L5, Moon's nadir, 1 SV in plane3	58	70.6	40	44.6	43	83
L5, Moon's nadir, 3 SVs in plane3	50	74.2	34	47.2	38	83.3
L4, L5, Moon's nadir, 1 SV in plane1	30	82.9	24	74	15	98.2
L4, L5, Moon's nadir, 3 SVs in plane1	13	92.3	15	88.1	10	98.8
L4, L5, Moon's nadir, 1 SV in plane2	19	89.5	23	83.1	23	96.8
L4, L5, Moon's nadir, 3 SVs in plane2	15	91.4	18	87.2	21	97.2
L4, L5, Moon's nadir, 1 SV in plane3	20	87.7	20	86.4	17	98.1
L4, L5, Moon's nadir, 3 SVs in plane3	17	91.2	16	87.8	11	98.5
L1, L4, L5, Moon's nadir, 1 SV in plane1	11	95.3	11	95.2	5	99.5
L1, L4, L5, Moon's nadir, 3 SVs in plane1	2	100	2	100	2	100
L1, L4, L5, Moon's nadir, 1 SV in plane2	7	97.9	8	98.6	19	98
L1, L4, L5, Moon's nadir, 3 SVs in plane2	6	99.2	6	99.1	14	98.4
L1, L4, L5, Moon's nadir, 1 SV in plane3	9	97	7	98.7	7	99.4
L1, L4, L5, Moon's nadir, 3 SVs in plane3	3	99.4	4	99.9	4	99.8
notional LEO nadir point	101	13.7	103	0	102	1.5
LEO nadir, L1	55	71.4	69	6.6	92	49.4
LEO nadir, L4	96	32	65	10.8	99	17.9
LEO nadir, L5	97	31.9	66	9.6	100	17.7
LEO nadir, Moon's nadir	95	36.1	68	7.7	97	31.1
LEO nadir, 1 SV in plane1	52	74	84	0.1	37	83.5
LEO nadir, 3 SVs in plane1	21	87.7	67	9.4	31	84.1

Bibliography

Bartels, M. (2019, October 23). *Israel Plans to Go Back to the Moon … And Stick the Landing This Time*. Retrieved from Space.com: https://www.space.com/israel-beresheet-moon-lander-try-again.html

Cheng, D. (2016, November 21). *China's move to cis-lunar space*. Retrieved from Space News Magazine: http://www.spacenewsmag.com/commentary/chinas-move-to-cis-lunar-space/

Department of Space, Indian Space Research Organisation. (2017). *CHANDRAYAAN: India's First Lunar Exploration Mission*. Retrieved from isro.gov: https://www.isro.gov.in/pslv-c11-chandrayaan-1

Fact Sheets: COBRA DANE Radar. (2017, 3 22). Retrieved from United States Space Force: https://www.spaceforce.mil/About-Us/Fact-Sheets/Article/2197716/cobra-dane-radar/

Hecht, E. (2016). *Optics (5th Edition).* Malaysia: Pearson Education Limited.

Jet Propulsion Laboratory. (2014, April 30). *Solar System Dynamics*. Retrieved 11 10, 2020, from JPL Planetary and Lunar Ephemerides: https://ssd.jpl.nasa.gov/?planet_eph_export

Knister, S. R. (2020). *Evaluation Framework for Cislunar Space Domain Awareness (SDA) Systems.* Air Force Institute of Technology, Department of Systems Engineering and Management. Wright-Patterson AFB: Air Force Institute of Technology.

MathWorks. (2020). *planetEphemeris*. Retrieved from Help Center: https://www.mathworks.com/help/aerotbx/ug/planetephemeris.html

National Aeronautics and Space Administration. (2020, September 16). *Explore Moon to Mars*. Retrieved from NASA: https://www.nasa.gov/topics/moon-to-mars/overview

The Planetary Society. (2020). *Chang'e-4: First lander and rover on the Moon's far side*. Retrieved from The Planetary Society: https://www.planetary.org/space-missions/change-4

Vendl, J. K. (2020). *Cislunar Periodic Orbit Analysis for Space Object Detection Capability*. University of Colorado, Department of Aerospace Engineering Sciences. Boulder: University of Colorado.

Wall, M. (2020, January 2). *India Is Officially Going Back to the Moon with Chandrayaan-3 Lunar Lander*. Retrieved from Space.com: https://www.space.com/india-confirms-moon-landing-mission-chandrayaan-3.html

Wiesel, W. E. (2010). *Modern Orbit Determination* (2nd ed.). Beavercreek, Ohio: Aphelion Press.

Wiesel, W. E. (2010). *Spaceflight Dynamics* (3rd ed.). Beavercreek, Ohio: Aphelion Press.

Xu, L. (2018, June 15). *How China's lunar relay satellite arrived in its final orbit*. Retrieved from The Planetary Society: https://www.planetary.org/articles/20180615-queqiao-orbit-explainer

REPORT DOCUMENTATION PAGE

Form Approved
OMB No. 074-0188

1. REPORT DATE *(DD-MM-YYYY)*	**2. REPORT TYPE**	**3. DATES COVERED** *(From – To)*
13-11-2020	Master's Thesis	April 2020 – November 2020

TITLE AND SUBTITLE

Assessing Observer Stations for Cislunar Space Domain Awareness

5a. CONTRACT NUMBER

5b. GRANT NUMBER

5c. PROGRAM ELEMENT NUMBER

6. AUTHOR(S)

Rosenof, Michael S., Major, USAF

5d. PROJECT NUMBER

5e. TASK NUMBER

5f. WORK UNIT NUMBER

7. PERFORMING ORGANIZATION NAMES(S) AND ADDRESS(S)
Air Force Institute of Technology
Graduate School of Engineering and Management (AFIT/ENY)
2950 Hobson Way, Building 640
WPAFB OH 45433-8865

8. PERFORMING ORGANIZATION REPORT NUMBER

AFIT-ENY-MS-20-D-068

9. SPONSORING/MONITORING AGENCY NAME(S) AND ADDRESS(ES)
Intentionally left blank

10. SPONSOR/MONITOR'S ACRONYM(S)

11. SPONSOR/MONITOR'S REPORT NUMBER(S)

12. DISTRIBUTION/AVAILABILITY STATEMENT
DISTRUBTION STATEMENT A. APPROVED FOR PUBLIC RELEASE; DISTRIBUTION UNLIMITED.

13. SUPPLEMENTARY NOTES
This material is declared a work of the U.S. Government and is not subject to copyright protection in the United States.

14. ABSTRACT

With renewed worldwide interest in cislunar space, the need for reliable domain awareness in that extended region of space is clear. This investigation quantifies the suitability of several possible stations for observer satellites in cislunar space by calculating the specific irradiance each would observe as they track satellites in various realistic lunar free-return trajectories across a decade, using reflected sunlight. This investigation includes one class of free return trajectories for target satellites, eleven distinct observer stations, and three different metrics for comparing the effectiveness of each observer station or combination of observer stations for sensing targets using reflected sunlight. The analysis showed that observer satellites in most, but not all, observer stations would be more effective than in low Earth orbit, and certain combinations of observer stations were significantly more effective. The exact ranking of least to most effective varied depending on the metric used.

15. SUBJECT TERMS
Cis-Lunar, Cislunar, Space Domain Awareness, Space Situational Awareness, Special Perturbations, 3-Body Problem, N-Body Problem, Astrodynamics, Astronautics, Moon, Solar System

16. SECURITY CLASSIFICATION OF:			**17. LIMITATION OF ABSTRACT**	**18. NUMBER OF PAGES**	**19a. NAME OF RESPONSIBLE PERSON**
a. REPORT	**b. ABSTRACT**	**c. THIS PAGE**			Lt Col Bryan D. Little, AFIT/ENY
U	**U**	**U**	**UU**	19	**19b. TELEPHONE NUMBER** *(Include area code)* (937) 255-3636, ext 4901 Bryan.Little@afit.edu

Standard Form 298 (Rev. 8-98)
Prescribed by ANSI Std. Z39-18